# Iron and nickel atoms in comet atmospheres

**Jean Manfroid** ( jmanfroid@gmail.com )
Institut d'Astrophysique et de Géophysique
**Damien Hutsemekers**
University of Liège
**Emmanuel Jehin**
Universite de Liege

**Physical Sciences - Article**

**Keywords:** Cometary Nuclei Sublimate, Remote Spectral Analysis, Sungrazer Comets, ESO Very Large Telescope

**Posted Date:** November 10th, 2020

**DOI:** https://doi.org/10.21203/rs.3.rs-101492/v1



**Version of Record:** A version of this preprint was published at Nature on May 19th, 2021. See the published version at https://doi.org/10.1038/s41586-021-03435-0.

# Iron and nickel atoms in comet atmospheres

J.Manfroid, D. Hutsemékers, and E. Jehin

STAR Institute, University of Liège

Allée du 6 Août 19c, B-4000 Liège, Belgium

November 1, 2020

**Abstract**

**When sufficiently close to the Sun, ices in cometary nuclei sublimate, ejecting in space dust and gases whose compositions can be derived by the remote spectral analysis of the cometary atmospheres. Those very rich spectra reveal a host of constituents from simple radicals like OH and CN in the optical range, to relatively complex organic molecules in the infrared and sub-millimeter domain. The majority of these molecules are made of C, H, O and N atoms. Iron, nickel and a few other siderophile atoms have only been detected in two exceptional sungrazer comets in a century and a half. Here we report that free atoms of iron and nickel are ubiquitous in cometary atmospheres as revealed by high-resolution spectra obtained in the near-ultraviolet with the ESO Very Large Telescope for a large sample of comets of various dynamical origins. The emissions of NiI and FeI in cometary comae have been overlooked until now and, surprisingly, are even detected at large heliocentric distances. The abundances of both species appear to be of the same order of magnitude, contrasting with the typical solar system abundance and providing clues about their origins in comet nuclei.**

The presence of iron in a comet atmosphere was discovered as early as the nineteenth century. Visual observations of the Great Comet of 1882 (C/1882 R1, 1882 II) had shown emission lines of iron, sodium and, possibly, of calcium and titanium [1]. The observations of this exceptional sungrazer comet were done during daytime with the 15-inch refractor at Lord Crawford's private observatory in Dun Echt (UK) when the comet was only at 0.098 au from the sun. Almost a century later, taking advantage of the passage of another very bright sungrazer comet, C/1965 S1 (Ikeya-Seki), iron, nickel, cobalt, copper, manganese, sodium and ionized calcium lines were recorded on photographic plates when the comet was at 0.14 au from the Sun [2–7]. Iron lines were predominant whereas nickel was much less

abundant, with a Ni/Fe ratio comparable to that of chondrites and the solar photosphere [5]. These two comets were the brightest ever observed through a telescope and the metals were detected at very short heliocentric distances. It could therefore be assumed that the appearance of these lines was related to the intense solar radiation at perihelion at only a few solar radii ($r$=0.0086 au and 0.0078 au, respectively) just hours before the observations. The equilibrium temperature exceeded 3000 K allowing to sublimate refractory materials such as metallic nickel and iron which are "moderately refractory" with condensation temperatures between 1300 and 1500 K [8].

The presence of iron vapor has also been claimed in another bright comet, C/2006 P1 (McNaught), based, not on spectroscopy but on the dynamical properties of a faint tail observed at perihelion ($r$ = 0.17 to 0.19 au) by the Heliospheric Imager aboard the STEREO spacecraft [9]. The iron atoms were thought to sublimate from sulfide grains, as direct ejection from refractories would be difficult at such perihelion distance (the solar radiation being about 500 times weaker than for the other two comets).

Nickel and iron were detected in refractory dust particles collected in the coma of comet 81P/Wild 2 by the NASA Stardust spacecraft and analysed on Earth [10, 11], and in situ by the COSIMA experiment of the Rosetta ESA mission to comet 67P/Churyumov-Gerasimenko [12, 13]. Infrared spectra of the ejecta plume of comet 9P/Tempel 1 obtained by the NASA's Spitzer space telescope during the Deep Impact encounter revealed amorphous and crystalline inorganic grains, including iron-rich olivines, pyroxene and smectite [14]. But up to now, no iron- or nickel-bearing molecules have been observed in the gaseous coma of comets, not even by the Rosetta spacecraft and its very sensitive mass spectrometer Rosina [15, 16].

In the last two decades we observed dozens of comets of various dynamical origins with the high-resolution Ultraviolet-Visual Echelle Spectrograph (UVES) of the ESO Very Large Telescope (VLT), in order to estimate, among other properties, their isotopic ratios and detailed compositions [17–19]. Our attention was drawn to a series of lines in the spectra of the peculiar comet C/2016 R2 (PanSTARRS) (Extended data Fig. 1). This peculiar comet is characterized by very low CN, $C_3$ and $C_2$ abundances [19] that allowed to identify more easily faint lines usually hidden in the forest of molecular features. These lines could be matched with the FeI and NiI tables from the National Institute of Standards and Technology (NIST) [20] and we decided to find out if they were present in other UVES spectra.

# 1 Results

The UVES VLT spectra used here (Extended data Table 1) were collected over a large range of heliocentric distances (0.68 au to 3.25 au). The use of a narrow 0.4 arcsec slit provides a resolving power ($\lambda/\Delta\lambda$) of about 80000 and its length of 10 arcsec covers ∼7500 km of the coma at a distance of 1.0 au. Except for a few cases the slit was centered on the comet nucleus. The use of a dichroic filter feeding the blue and red arms of the spectrograph allowed to obtain for most comets a spectrum covering a large part of the spectral range from the near UV atmospheric cutoff to the near IR (304-1040 nm). The reduction procedure is similar to that of [21].

Close examination of these spectra revealed the omnipresence of iron and nickel, with up to about 40 FeI lines and 25 NiI lines in some of them. A complete list of the FeI and NiI lines positions and intensities identified for each comet can be found as Supplementary information (FN-lines.csv). These lines are located in the blue part of the spectrum ($< 450$ nm) where there are plenty of bright molecular emissions making blends unavoidable. Examples are the bright FeI 3859.91 Å and 3856.37 Å lines which are blended with the generally much stronger CN R4 3859.95 Å and R9 3856.40 Å, respectively, as well as the NiI 3458.46 Å line which is often overwhelmed by some underlying line, explaining in part why they were missed until now. We searched for the lines of the other atoms of the iron peak that were observed in comet Ikeya-Seki, in particular neutral chromium, the most abundant after nickel, but we could not identify any of them.

The metallic lines, contrary to the molecular lines, are sharp and peaked on the nucleus with only a short spatial extension as it was already noted by [5] for Ikeya-Seki. The few spectra not centered on the nucleus do not show these lines, or only faintly. The best lines in the spectra obtained during the relatively close encounter of 103P/Hartley 2 with the Earth (Extended data, Fig. 1) show a radiance inversely proportional to the distance to the nucleus $p$. Such a profile corresponds to an ejection from the surface of the nucleus or a short-lived parent [3] and a constant expansion velocity, resulting in a $1/p^2$ density distribution. The spectra taken parallel and perpendicular to the Sun direction indicate that the metal distribution in the inner coma is isotrope. This suggests collisional dragging and an initial velocity high enough to hide radiative pressure effects.

# 2 Analysis

Once freed in a collision-less environment, the atoms are bathed into the solar radiation and would conceivably tend toward an excitation temperature of the order of the effective temperature of the Sun,

about 5800 K. In order to analyze their emission spectra, we first considered a simple 3-level model as done previously for the analysis of Ikeya-Seki [2, 22]. Since this model is based on several assumptions and simplifications, we also built a multilevel atomic model taking into account the complex high-resolution structure of the solar spectrum (Section 4.1 in Methods). This yields column densities which allowed us to compute the production rates of NiI and FeI for each comet.

The column density profile is derived from the average over the slit area by means of a $1/p$ distribution convolved with a 1 arcsec gaussian representing the typical seeing. In the case of an isotropic expansion at a constant velocity $v$, the column densities $N_{\rm col}$ and the production rates $Q$ are linked by the relation $N_{\rm col} = Q/(4v\Delta p)$. We adopt the commonly assumed value of 0.85 $r^{-1/2}$ km/s [23] for the expansion velocity of both atoms. Table 2 (Extended data) gives for each spectrum the FeI and NiI column densities and production rates.

In order to compare these abundances with the other species observed in our spectra, we calculate the production rates of OH, CN and $CO_2^+$ using Haser models [24–27] integrated over the slit (Extended data, Table 3). As a proxy to the dust production rate we use the $Af\rho$ parameter [28], to which it is proportional for a $1/p$ brightness profile. $Af\rho$ is derived from the dust continuum intensity around the CN band and is corrected for the phase effect, the seeing and the slit geometry. The comparison with the production rates of OH, $H_2O$, CO, CN, $CO_2^+$ and the dust (Extended data, Fig. 9) shows that the production rates of FeI and NiI are well correlated with those species, with the neat exception of comet C/2016 R2 for which NiI and FeI correlates only with CO and $CO_2^+$.

The quantities found are very small. For the Jupiter family comets they correspond to only about 1 g of metal ejected every second, compared to about 100 kg of water, making these elements minor constituents of the coma.

The Ni/Fe abundance ratio does not depend on the heliocentric distance or the comet origin (Fig. 2). Its average value is about unity ($\log(\mathrm{Ni/Fe}) = -0.06 \pm 0.31$), i.e., an order of magnitude higher than the solar value ($\log(\mathrm{Ni/Fe}) = -1.25 \pm 0.04$, [29]) and the ratio measured in Ikeya-Seki ($\log(\mathrm{Ni/Fe}) = -1.11 \pm 0.09$). In our sample, comet 103P/Hartley 2 has the lowest value, $\log(\mathrm{Ni/Fe}) = -0.64 \pm 0.07$, and the carbon-chain depleted comet 73P the highest value, $\log(\mathrm{Ni/Fe}) = 0.60 \pm 0.23$, both at heliocentric distances close to 1 au.

# 3 Discussion

The key result of this study is the detection of ubiquitous FeI and NiI emission lines in a large sample of comets up to heliocentric distances as far as 3 au, with an average Ni/Fe abundance ratio of about 1, much higher than in the sungrazer comet Ikeya-Seki, and than in the Sun. Another important result is the high metallic abundance in the distant and chemically peculiar comet C/2016 R2 relative to its other elements, except CO and $CO_2^+$. This water-poor comet had a high activity driven by a large CO production rate of about $10^{29}$ molecules/s [31, 32]. The spatial profile of the metal lines indicates that the atoms must originate directly from the nucleus, or from some parent which dissipates rapidly.

The comet blackbody equilibrium temperature is expected to be around $T \simeq 280\ r^{-1/2}$ K with $r$ in au, that is ∼340 K for the comet observed at the closest distance to the Sun (0.68 au) and ∼150 K for the most distant one (3.3 au). These temperatures are much lower than those required to vaporize refractory dust grains or iron and nickel in metallic form. We thus explore several possibilities to explain how FeI and NiI atoms are released at such low temperatures and why nickel is enhanced by an order of magnitude relative to iron compared to the solar system abundances.

The radiation pressure on the iron atoms is relatively small. The $\beta$-parameter characterizing the ratio between the radiation pressure and the gravity is about 6 for iron [9], which is too small to alter appreciably the velocity field in the vicinity of the nucleus and to significantly decrease the column density of iron relatively to nickel. Moreover, comet Ikeya-Seki which should show the largest effects, displays a normal (solar) abundance ratio. The observed high Ni/Fe ratio must then be representative of the sublimating material or of the sublimation process.

Iron is known to be distributed between silicates, sulfides and metallic iron, silicates and metallic iron requiring much higher temperatures (∼ 1200 K) to sublimate than sulfides (∼ 600 K), while nickel is only found in sulfides and the metal phase [33, 34]. We may thus naturally expect a higher Ni/Fe abundance ratio if sublimation occurs at temperatures lower than 1000 K. This is even more true as the FeNi alloys and sulfides formed in the low temperature range are Ni-rich, such as kamacite and pentlandite [35]. Although some comets might actually be Ni-rich, partial sublimation of species with Ni/Fe solar abundances could thus explain the high Ni/Fe abundance ratios we measure in comets far enough from the Sun. This nevertheless requires temperatures around 500 K at least, still higher than expected from the blackbody equilibrium temperature at heliocentric distances larger than 0.4 au. FeNi metals and Ni-rich sulfides like pentlandite have been found in cometary material and interplanetary dust particles (IDPs), often in the form of nanometer-sized particles [36–39]. The number of Fe and

Ni atoms beeing the same, it would offer a clear explanation for the relative abundance close to 1, in average, but not the large over- or under-abundance of Ni, observed in, e.g., comets Garradd and Hartley 2, or in the carbon-chain depleted comets 21P and 73P.

Small cometary grains can be heated to much higher temperatures than blackbody equilibrium temperatures [40], especially if they are small enough to be stochastically heated [41]. Collisions of high-velocity nanoparticles with cometary dust grains could break the matrix in which Fe and Ni are embedded and produce impact vapor with a temperature that could be of the order of 1000 K [42]. Several mechanisms can thus potentially provide the necessary heating, especially if a significant amount of iron and nickel is in the form of nanoparticles.

The correlation of the production rates of iron, nickel and carbon oxydes for all the comets of our sample may point to some common origin. Iron and nickel carbonyls, $Fe(CO)_5$ and $Ni(CO)_4$, respectively, have been proposed as possible cometary constituents [43, 44]. To test this hypothesis we have estimated the sublimation temperatures and sublimation rates of both the iron and nickel carbonyls (Methods 4.2). These temperatures are only slightly higher than that of $CO_2$ and indicate that, if present in comets, these carbonyls can sublimate at low temperatures and at large distances from the Sun, contrary to the silicates and sulfides. This could explain why carbonyls have not been found in IDPs while they have been recently identified in the Lewis Cliff 85311 meteorite [45]. Furthermore the higher rate of sublimation of $Ni(CO)_4$ compared to $Fe(CO)_5$ (Fig 3), about a factor 10 at temperatures around 300 K typical of the diurnal temperature of the nucleus [46], might provide a simple explanation to the Ni/Fe overabundance. This scenario nevertheless depends on the efficiency of the photodissociation of the carbonyls. Interestingly, similar computations for chromium, the next most abundant metal in the Sun after Ni, show that the sublimation rate of $Cr(CO)_6$ is lower by a factor of about 100 with respect to $Fe(CO)_5$, which means that, if both CrI and FeI originate from carbonyls, CrI would be a factor of about 10000 less abundant than FeI, explaining the non detection of the CrI lines. A detailed photochemical analysis, beyond the scope of this paper, would be needed to verify if this scenario can actually reproduce the measured abundances, but the discovery of iron and nickel free atoms in comets indicates that important constituents of the nucleus or processes in the coma are still missing, possibly bringing new important constraints on comets composition and the solar system formation.

# References


[1]R. Copeland and J. G. Lohse, "Spectroscopic observations of comets III and IV, 1881, comet I, 1882, and the Great Comet of 1882", Copernicus: an International Journal of Astronomy **2**, 225–244 (1882).

[2]C. Arpigny, "Relative abundances of the heavy elements in comet Ikeya-Seki /1965 VIII/", in Liege international astrophysical colloquia, Vol. 22, edited by A. Boury, N. Grevesse, and L. Remy-Battiau, Liege International Astrophysical Colloquia (Jan. 1979), pp. 189–197.

[3]M. R. Combi, M. A. DiSanti, and U. Fink, "The Spatial Distribution of Gaseous Atomic Sodium in the Comae of Comets: Evidence for Direct Nucleus and Extended Plasma Sources", Icarus **130**, 336–354 (1997).

[4]J. Dufay, P. Swings, and C. Fehrenbach, "Spectrographic Observations of Comet Ikeya-Seki (1965f).", ApJ **142**, 1698 (1965).

[5]G. W. Preston, "The spectrum of Ikeya-Seki (1965f)", ApJ **147**, 718–742 (1967).

[6]C. D. Slaughter, "The Emission Spectrum of Comet Ikeya-Seki 1965-f at Perihelion Passage", AJ **74**, 929 (1969).

[7]A. D. Thackeray, M. W. Feast, and B. Warner, "Daytime Spectra of Comet Ikeya-Seki Near Perihelion", ApJ **143**, 276 (1966).

[8]S. R. Taylor, *Solar system evolution: a new perspective*, 2nd ed. (Cambridge University Press, 2001).

[9]M. Fulle, F. Leblanc, R. A. Harrison, C. J. Davis, C. J. Eyles, J. P. Halain, R. A. Howard, D. Bockelée-Morvan, G. Cremonese, and T. Scarmato, "Discovery of the Atomic Iron Tail of Comet MCNaught Using the Heliospheric Imager on STEREO", ApJ **661**, L93–L96 (2007).

[10]D. Brownlee, "The Stardust Mission: Analyzing Samples from the Edge of the Solar System", Annual Review of Earth and Planetary Sciences **42**, 179–205 (2014).

[11]Z. Gainsforth, A. J. Westphal, A. L. Butterworth, C. E. Jilly-Rehak, D. E. Brownlee, D. J. Joswiak, R. C. Ogliore, M. E. Zolensky, H. A. Bechtel, D. S. Ebel, G. R. Huss, S. A. Sandford, and A. J. White, "Fine-grained material associated with a large sulfide returned from Comet 81P/Wild 2", Meteoritics and Planetary Science **54**, 1069–1091 (2019).

[12]O. J. Stenzel, M. Hilchenbach, S. Merouane, J. Paquette, K. Varmuza, C. Engrand, F. Brand stätter, C. Koeberl, L. Ferrière, P. Filzmoser, and S. r. Siljeström, "Similarities in element content between

comet 67P/Churyumov-Gerasimenko coma dust and selected meteorite samples", MNRAS **469**, S492–S505 (2017).

[13]A.-C. Levasseur-Regourd, J. Agarwal, H. Cottin, C. Engrand, G. Flynn, M. Fulle, T. Gombosi, Y. Langevin, J. Lasue, T. Mannel, S. Merouane, O. Poch, N. Thomas, and A. Westphal, "Cometary Dust", Space Sci. Rev. **214**, 64, 64 (2018).

[14]C. M. Lisse, J. VanCleve, A. C. Adams, M. F. A'Hearn, Y. R. Fernández, T. L. Farnham, L. Armus, C. J. Grillmair, J. Ingalls, M. J. S. Belton, O. Groussin, L. A. McFadden, K. J. Meech, P. H. Schultz, B. C. Clark, L. M. Feaga, and J. M. Sunshine, "Spitzer Spectral Observations of the Deep Impact Ejecta", Science **313**, 635–640 (2006).

[15]A. L. Cochran, A.-C. Levasseur-Regourd, M. Cordiner, E. Hadamcik, J. Lasue, A. Gicquel, D. G. Schleicher, S. B. Charnley, M. J. Mumma, L. Paganini, D. Bockelée-Morvan, N. Biver, and Y.-J. Kuan, "The Composition of Comets", Space Sci. Rev. **197**, 9–46 (2015).

[16]M. Rubin, K. Altwegg, H. Balsiger, J.-J. Berthelier, M. R. Combi, J. De Keyser, M. Drozdovskaya, B. Fiethe, S. A. Fuselier, S. Gasc, T. I. Gombosi, N. Hänni, K. C. Hansen, U. Mall, H. Rème, I. R. H. G. Schroeder, M. Schuhmann, T. Sémon, J. H. Waite, S. F. Wampfler, and P. Wurz, "Elemental and molecular abundances in comet 67P/Churyumov-Gerasimenko", MNRAS **489**, 594–607 (2019).

[17]J. Manfroid, E. Jehin, D. Hutsemékers, A. Cochran, J. .-M. Zucconi, C. Arpigny, R. Schulz, J. A. Stüwe, and I. Ilyin, "The CN isotopic ratios in comets", A&A **503**, 613–624 (2009).

[18]A. Decock, E. Jehin, P. Rousselot, D. Hutsemékers, J. Manfroid, S. Raghuram, A. Bhardwaj, and B. Hubert, "Forbidden oxygen lines at various nucleocentric distances in comets", A&A **573**, A1, A1 (2015).

[19]C. Opitom, D. Hutsemékers, E. Jehin, P. Rousselot, F. J. Pozuelos, J. Manfroid, Y. Moulane, M. Gillon, and Z. Benkhaldoun, "High resolution optical spectroscopy of the $N_2$-rich comet C/2016 R2 (PanSTARRS)", A&A **624**, A64, A64 (2019).

[20]A. Kramida, Yu. Ralchenko, J. Reader, and and NIST ASD Team, edited by N. I. of Standards and M. Technology Gaithersburg, NIST Atomic Spectra Database (ver. 5.7.1),`https://physics.nist.gov/asd` [2019, November 29], 2019.

[21]C. Arpigny, E. Jehin, J. Manfroid, D. Hutsemékers, R. Schulz, J. A. Stüwe, J.-M. Zucconi, and I. Ilyin, "Anomalous Nitrogen Isotope Ratio in Comets", Science **301**, 1522–1525 (2003).

[22]C. Arpigny, "On the nature of comets.", in Proceedings of the robert a. welch foundation conferences on chemical research xxi, cosmochemistry, edited by W. Mulligan (1978), p. 9.

[23]A. L. Cochran and D. G. Schleicher, "Observational Constraints on the Lifetime of Cometary H $_2$O", Icarus **105**, 235–253 (1993).

[24]M. F. A'Hearn, R. C. Millis, D. O. Schleicher, D. J. Osip, and P. V. Birch, "The ensemble properties of comets: Results from narrowband photometry of 85 comets, 1976-1992.", Icarus **118**, 223–270 (1995).

[25]A. Bhardwaj and S. Raghuram, "A Coupled Chemistry-emission Model for Atomic Oxygen Green and Red-doublet Emissions in the Comet C/1996 B2 Hyakutake", ApJ **748**, 13, 13 (2012).

[26]L. Haser, "Distribution d'intensité dans la tête d'une comète", Bulletin de la Societe Royale des Sciences de Liege **43**, 740–750 (1957).

[27]S. J. Kim, "Fluorescence efficiencies of the A-X and B-X systems of $CO_2^+$ in comets", Earth, Planets, and Space **51**, 139–145 (1999).

[28]M. F. A'Hearn, D. G. Schleicher, R. L. Millis, P. D. Feldman, and D. T. Thompson, "Comet Bowell 1980b", AJ **89**, 579–591 (1984).

[29]K. Lodders, "Solar Elemental Abundances", arXiv e-prints, arXiv:1912.00844 (2019).

[30]H. F. Levison, "Comet Taxonomy", in Completing the inventory of the solar system, Vol. 107, edited by T. Rettig and J. M. Hahn, Astronomical Society of the Pacific Conference Series (Jan. 1996), pp. 173–191.

[31]N. Biver, D. Bockelée-Morvan, M. Hofstadter, E. Lellouch, M. Choukroun, S. Gulkis, J. Crovisier, F. P. Schloerb, L. Rezac, P. von Allmen, S. Lee, C. Leyrat, W. H. Ip, P. Hartogh, P. Encrenaz, G. Beaudin, and Miro Team, "Long-term monitoring of the outgassing and composition of comet 67P/Churyumov-Gerasimenko with the Rosetta/MIRO instrument", A&A **630**, A19, A19 (2019).

[32]M. Womack, G. Sarid, and K. Wierzchos, "CO in Distantly Active Comets", PASP **129**, 031001 (2017).

[33]J. W. Larimer and E. Anders, "Chemical fractionations in meteorites - III. Major element fractionations in chondrites", Geochim. Cosmochim. Acta **34**, 367–387 (1970).

[34]L. Grossman and J. W. Larimer, "Early chemical history of the solar system.", Reviews of Geophysics and Space Physics **12**, 71–101 (1974).

[35]J. S. Lewis, *Physics and chemistry of the solar system. 2nd Edition* (2004).

[36]E. L. Berger, T. J. Zega, L. P. Keller, and D. S. Lauretta, "Evidence for aqueous activity on comet 81P/Wild 2 from sulfide mineral assemblages in Stardust samples and CI chondrites", Geochim. Cosmochim. Acta **75**, 3501–3513 (2011).

[37]J. P. Bradley, "Chemically Anomalous, Preaccretionally Irradiated Grains in Interplanetary Dust From Comets", Science **265**, 925–929 (1994).

[38]H. A. Ishii, J. P. Bradley, Z. R. Dai, M. Chi, A. T. Kearsley, M. J. Burchell, N. D. Browning, and F. Molster, "Comparison of Comet 81P/Wild 2 Dust with Interplanetary Dust from Comets", Science **319**, 447 (2008).

[39]M. E. Zolensky, T. J. Zega, H. Yano, S. Wirick, A. J. Westphal, M. K. Weisberg, I. Weber, J. L. Warren, M. A. Velbel, A. Tsuchiyama, P. Tsou, A. Toppani, N. Tomioka, K. Tomeoka, N. Teslich, M. Taheri, J. Susini, R. Stroud, T. Stephan, F. J. Stadermann, C. J. Snead, S. B. Simon, A. Simionovici, T. H. See, F. Robert, F. J. M. Rietmeijer, W. Rao, M. C. Perronnet, D. A. Papanastassiou, K. Okudaira, K. Ohsumi, I. Ohnishi, K. Nakamura-Messenger, T. Nakamura, S. Mostefaoui, T. Mikouchi, A. Meibom, G. Matrajt, M. A. Marcus, H. Leroux, L. Lemelle, L. Le, A. Lanzirotti, F. Langenhorst, A. N. Krot, L. P. Keller, A. T. Kearsley, D. Joswiak, D. Jacob, H. Ishii, R. Harvey, K. Hagiya, L. Grossman, J. N. Grossman, G. A. Graham, M. Gounelle, P. Gillet, M. J. Genge, G. Flynn, T. Ferroir, S. Fallon, D. S. Ebel, Z. R. Dai, P. Cordier, B. Clark, M. Chi, A. L. Butterworth, D. E. Brownlee, J. C. Bridges, S. Brennan, A. Brearley, J. P. Bradley, P. Bleuet, P. A. Bland, and R. Bastien, "Mineralogy and Petrology of Comet 81P/Wild 2 Nucleus Samples", Science **314**, 1735 (2006).

[40]M. S. Hanner, "Effect of the size distribution on the thermal emission from cometary dust", in The comet halley. dust and gas environment, Vol. 174, edited by B. Battrick and E. Swallow, ESA Special Publication (Nov. 1981), pp. 67–75.

[41]B. S. Hensley and B. T. Draine, "Thermodynamics and Charging of Interstellar Iron Nanoparticles", ApJ **834**, 134, 134 (2017).

[42]W. .-H. Ip and L. Jorda, "Can the Sodium Tail of Comet Hale-Bopp Have a Dust-Impact Origin?", ApJ **496**, L47–L49 (1998).

[43]M. R. Bloch and H. L. Wirth, "Abiotic organic synthesis in space", Naturwissenschaften **67**, 562–564 (1980).

[44]W. F. Huebner, "Dust from cometary nuclei", A&A **5**, 286–297 (1970).

[45]K. E. Smith, C. H. House, R. D. Arevalo, J. P. Dworkin, and M. P. Callahan, "Organometallic compounds as carriers of extraterrestrial cyanide in primitive meteorites", Nature Communications **10**, 2777, 2777 (2019).

[46]D. Prialnik, J. Benkhoff, and M. Podolak, "Modeling the structure and activity of comet nuclei", in *Comets ii*, edited by M. C. Festou, H. U. Keller, and H. A. Weaver (2004), p. 359.

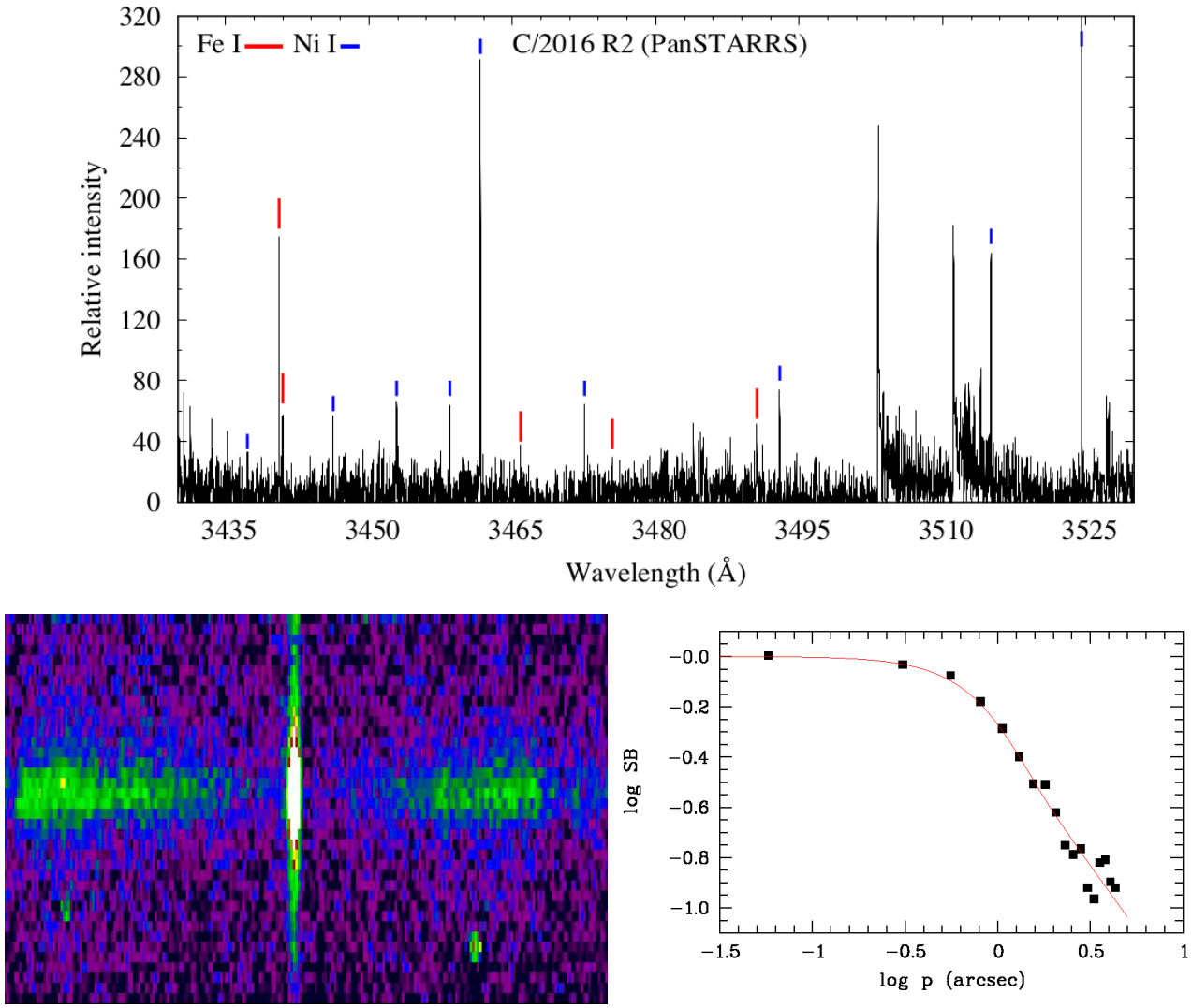


Figure 1: **Observations of the Fe and Ni lines.**
Top. C/2016 R2 spectrum. Selected region showing many FeI and NiI lines in the spectrum of comet C/2016 R2 (PanSTARRS) obtained at the ESO Very Large Telescope.
Bottom. The left panel shows the 2-dimensional spectrum of the FeI 3719 Å line in comet 103P/Hartley 2 on November 2010, at its closest approach to Earth at only 0.17 au. Wavelengths are along the horizontal axis and cover a range of 3 Å. The spatial dimension (vertical axis) extends over the entire height of the 10 arcsec slit (1230 km at the distance of the comet). The horizontal trace represents the reflected solar spectrum by the dust which shows a deep FeI absorption line. The spatial profile (right panel) plotted as a function of the projected nucleocentric distance $p$ agrees well with a $1/p$ distribution of the surface brightness and a 1.35 arcsec blurring corresponding to the seeing and the tracking imperfections. The NiI lines display the same profile.

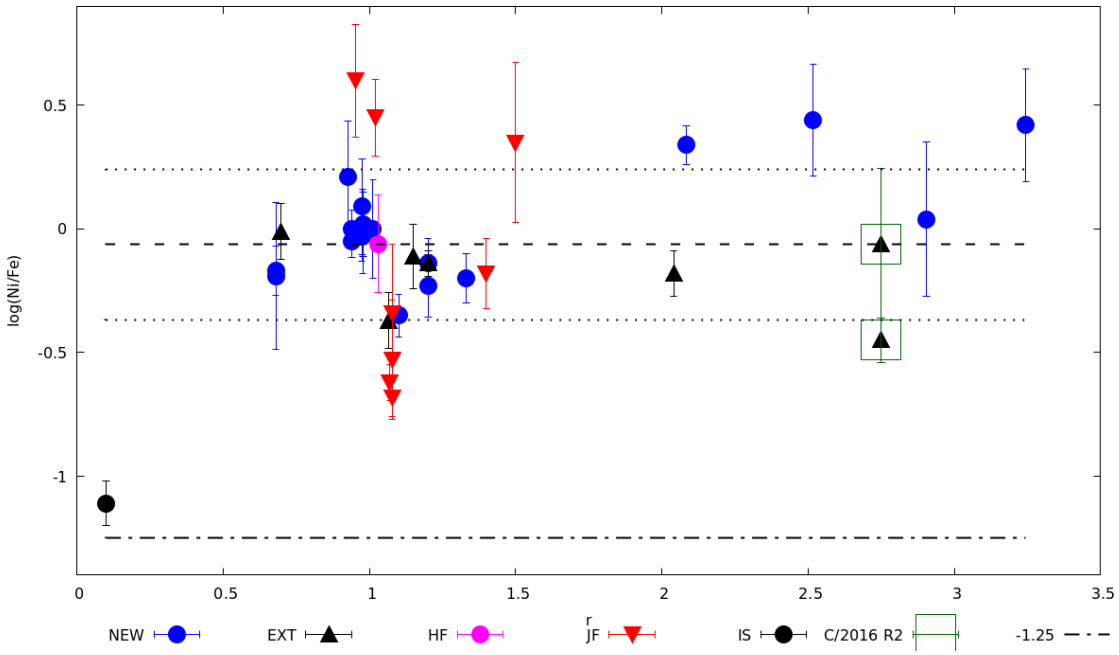


Figure 2: **Abundance ratios.**
Ni/Fe abundance ratios determined with the multilevel model for the comets of our sample. $r$ is the heliocentric distance. Different symbols are used according to the dynamical class [30] : HFC (Halley Family) and JFC (Jupiter Family) correspond to ecliptic comets with short periods (< 200 years), EXT corresponds to external comets with semi-major axis $a < 10000$ au and NEW corresponds to external comets which directly come from the Oort cloud ($a > 10000$ au). The great comet C/1965 S1 (Ikeya-Seki) has been added. The horizontal dashed-dotted line indicates the solar value. The dashed and the dotted lines represent the sample average and the standard deviation.

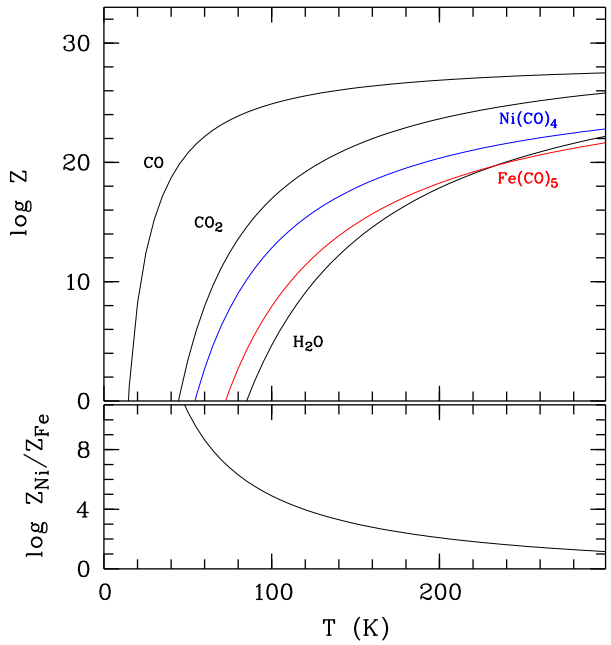


Figure 3: **Sublimation of carbonyls.**
Top : the sublimation rate (in molecules $cm^{-2}$ $s^{-1}$) of iron and nickel carbonyls as a function of the temperature, compared to major species in comets.
Bottom : the sublimation rate ratio $Ni(CO)_4$ over $Fe(CO)_5$.

# 4 Methods

## 4.1 Excitation of FeI and NiI lines by resonance fluorescence and determination of Ni/Fe abundance ratios

Preston [1] found that the intensity of the FeI and NiI emission lines observed in comet Ikeya-Seki at 0.14 au from the Sun can be related to the energy of the upper level of the transitions through a Boltzmann distribution, and that these lines are likely formed by resonance fluorescence. A simple "curve-of-growth" analysis then provided the excitation temperature of the lines and allowed the determination of the Ni/Fe abundance ratio. In Sect. 4.1.1, we explicitly reformulate the resonance fluorescence model [2, 3] considering a 3-level atom and assuming that the solar radiation can be represented by a diluted blackbody. For each comet the excitation temperature is empirically determined following Eq. 14 using the observed FeI emission line intensities and atomic data from the Atomic Line List v2.05 [4]. Suspected blends are not considered and a few recurrent outliers are discarded from the analysis, in particular a few FeI lines with lower energy levels higher than 2 eV, and the two NiI lines with the smallest $\log(gf)$. For NiI, the smaller range of upper energy levels precludes an accurate determination of the excitation temperature but, given the similar atomic level structure of FeI and NiI, we assume $T(\mathrm{NiI}) = T(\mathrm{FeI})$ as in [1–3]. In two comets, the number of observed FeI lines is too small to derive the temperature and we adopt $T = 4000 \pm 1000$ K, which is representative of the sample. The Ni/Fe abundance ratio is finally obtained from Eq. 15 with $\log U_{\mathrm{Ni}}/U_{\mathrm{Fe}} = 0.06 \pm 0.02$ computed for the temperature range 3500-5000 K. Errors on the abundance ratios account for the dispersion of the $C$ values (fixed to 0.3 dex when the line number is smaller than 3) and the range of acceptable temperatures. The metallic lines found in comet Ikeya-Seki were similarly analyzed[1], only considering the FeI and NiI lines that are also detected in our spectra to avoid any bias. Results for all comets are given in Sect. 4.1.1. The Ni/Fe abundance ratio derived for Ikeya-Seki is in excellent agreement with previous studies [1–3].

Although the 3-level model seems to provide a reasonably good interpretation of the FeI and NiI emission spectrum, it is based on approximations that need to be tested, in particular the assumption of identical excitation temperatures for FeI and NiI lines, and the use of a blackbody for the solar radiation (strong metallic lines in absorption are known to sprinkle the solar spectrum). We therefore built a multilevel atomic model where the true solar spectrum is taken into account. The model is described

[1] The line intensities are taken from [1]. This paper provides equivalent widths in units of the sky spectrum intensity and argues that the sky spectrum is mostly independent of wavelength ("white") so that the equivalent widths can be used as intensities with an error that can be as high as 30%.

in Sect. 4.1.2. Input atomic data are extracted from the Atomic Line List v2.05 [4]. For FeI, we consider transitions with lower levels in the energy range 0-20000 $cm^{-1}$, upper levels in the energy range 0-40000 $cm^{-1}$, and line strengths with $A_{ki} > 10^3$ $s^{-1}$. This results in 427 transitions with wavelengths between 2500 Å and 13000 Å for 85 energy levels including the ground level. For NiI, we use the same constraints with upper levels in the energy range 0-50000 $cm^{-1}$ [5]. For the solar spectrum, we use the calibrated high-resolution spectrum of [6]. The spectral range is 2960-13000 Å, with a resolving power between 350000 (UV) and 500000 (IR). For the spectral range 2000-2960 Å, we use the calibrated solar spectrum of [7] which has a lower spectral resolution of 0.1 Å. Results are presented in Sect. 4.1.2. The multilevel resonance fluorescence model reproduces fairly well the observations, although with a line by line dispersion that can be significant for some comets. The derived Ni/Fe abundance ratios are given in Table 2 (Extended data). Tests and possible improvements are discussed in Sect. 4.1.3, essentially showing that the measured abundance ratios are robust. In Sect. 4.1.4, we compare the results from the two models. First we show that the excitation temperatures systematically lower than the Sun color temperature can be explained by the presence of strong absorptions in the true solar spectrum. We also emphasize the importance of the comet heliocentric velocity as the cometary FeI and NiI transitions can sample very different portions of the solar spectrum depending of the Doppler shift. The abundance ratios computed with the 3-level model are in good agreement with those ones derived from the multilevel model but show a systematic shift of 0.2 dex that can be corrected taking $T(\mathrm{NiI}) = T(\mathrm{FeI})+180$ K.

### 4.1.1 Three-level atom

In addition to the ground level, FeI and NiI show a few metastable lower levels and upper levels of opposite parity. Observed transitions occur between the two sets of levels [2, 3, 5]. We then consider a 3-level atom, excited by resonance fluorescence. Statistical equilibrium for the ground and the lower levels writes

$$n_l(A_{lg} + B_{lg}J_{lg}) + n_u(A_{ug} + B_{ug}J_{ug}) = n_g(B_{gl}J_{gl} + B_{gu}J_{gu}) , \quad (1)$$

$$n_g(B_{gl}J_{gl}) + n_u(A_{ul} + B_{ul}J_{ul}) = n_l(A_{lg} + B_{lg}J_{lg} + B_{lu}J_{lu}) , \quad (2)$$

where $n_g$, $n_l$, and $n_u$ are the volume density of atoms in the ground, lower, and upper levels, respectively. $A$, $B$ are the Einstein coefficients and $J$ the mean intensity of the radiation. $J_{ij} = \int J(\nu)\,\phi(\nu)\,d\nu$ over the natural line profile that is $J_{ij} \simeq J(\nu_{ij})$ with $\int \phi(\nu)\,d\nu = 1$. Since the lower level is metastable,

transitions $g \leftrightarrow l$ can be neglected and these relations simplify to

$$\frac{n_u}{n_g} = \frac{B_{gu} J_{gu}}{(A_{ug} + B_{ug} J_{ug})} , \quad (3)$$

$$\frac{n_u}{n_l} = \frac{B_{lu} J_{lu}}{(A_{ul} + B_{ul} J_{ul})} . \quad (4)$$

With $A_{ui}/B_{ui} = 2h\nu_{ui}^3/c^2$ and $g_i B_{iu} = g_u B_{ui}$ for $i = g, l$, and assuming $J_\nu = W B_\nu$ where $B_\nu(T) = (2h\nu^3/c^2)/(e^{h\nu/kT} - 1)$ represents the solar blackbody radiation and $W$ the dilution factor

$$W = \frac{1}{2}(1 - \sqrt{1 - \frac{R_\odot^2}{r^2}}) \simeq \frac{1}{4}\frac{R_\odot^2}{r^2} , \quad (5)$$

we derive

$$\frac{n_u}{n_i} = \frac{g_u}{g_i} \frac{1}{1 + (e^{h\nu_{iu}/kT} - 1)/W} . \quad (6)$$

Since $W \ll 1$ and assuming $h\nu \gg kT$ (Wien approximation) we can finally write

$$n_u/n_g = W\,(g_u/g_g)\,10^{-\theta\,\chi_u} , \quad (7)$$

$$n_u/n_l = W\,(g_u/g_l)\,10^{-\theta\,(\chi_u - \chi_l)} , \quad \text{and then} \quad (8)$$

$$n_l/n_g = (g_l/g_g)\,10^{-\theta\,\chi_l} \quad (9)$$

where $\theta = 5040$ K / $T$ and $\chi_u$ ($\chi_l$) is the energy of the upper (lower) level in eV. If $n$ is the volume density of the atom in all states, $n_l/n = g_l 10^{-\theta\,\chi_l}/U(T)$ where $U(T) = \sum n_i$ is the partition function, so that we have

$$\frac{n_u}{n} = W \frac{g_u 10^{-\theta\,\chi_u}}{U(T)} . \quad (10)$$

Due to the dilution of exciting radiation, the upper levels are weakly populated with respect to the lower ones and $U(T) = \sum n_i \simeq g_g + \sum_l g_l 10^{-\theta\,\chi_l}$.

The intensity of the radiation emitted in the transition $u \to l$, integrated over the line of sight, is given by

$$I_\nu = \int j_\nu\, ds \qquad \text{where} \qquad j_\nu = \frac{1}{4\pi} n_u\, A_{ul}\, h\nu_{ul}\, \phi(\nu) . \quad (11)$$

Using the oscillator strength

$$f_{lu} = \frac{mc^3}{8\pi^2 e^2 \nu_{ul}^2} \frac{g_u}{g_l} A_{ul} \quad (12)$$

we write

$$I_\nu = N\,W\,\frac{8\pi^2 e^2 h}{4\pi m}\,\frac{g_l\,f_{lu}}{\lambda_{ul}^3}\,\frac{10^{-\theta\chi_u}}{U(T)}\,\phi(\nu) \tag{13}$$

where $N = \int n\,ds$ is the column density. This relation can be written in the form

$$\log\frac{I\lambda^3}{gf} = -\theta\,\chi_u + C \tag{14}$$

that allows the empirical determination of $\theta$ by plotting $\log(I\lambda^3/gf)$ against $\chi_u$ for observed spectral lines. $I = \int I_\nu\,d\nu = \int I_\lambda\,d\lambda$ is the intensity (surface brightness) integrated over the observed line profile. Relative abundances of two atoms 1 and 2 can then be obtained using

$$\log\frac{N_1}{N_2} = (C_1 - C_2) + \log\frac{U_1}{U_2}\,, \tag{15}$$

where the constant $C_i$ are computed from Eq. 14 for each observed line of a given atom using the derived value of $\theta$, and then averaged.

Fig. 4 illustrates for two comets the empirical method used to estimate the excitation temperature. In Table 2 we give the Ni/Fe abundance ratio computed with the 3-level model. $T$ is the excitation temperature used for both FeI and NiI, and $\mathrm{n_{lines}}$ the number of FeI and NiI lines considered in the analysis.

### 4.1.2 Multilevel atom

We consider $m$ energy levels. Statistical equilibrium for level $i$ reads

$$\sum_{\substack{j=1\\ j\neq i}}^{m} n_j\,Q_{ji} \;=\; n_i \sum_{\substack{j=1\\ j\neq i}}^{m} Q_{ij} \tag{16}$$

where $Q_{ij} = B_{ij}J_{ij}$ for $i < j$, $Q_{ij} = A_{ij} + B_{ij}J_{ij}$ and $A_{ij} = B_{ij}\,(2h\nu_{ij}^3/c^2)$ for $i > j$, and $g_iB_{ij} = g_jB_{ji}$. By defining $Q_{ii} = -\sum_{\substack{j=1\\ j\neq i}}^{m} Q_{ij}$ and $n'_j = n_j/n_1$, we finally have for level $i$

$$\sum_{j=2}^{m} n'_j\,Q_{ji} \;=\; -Q_{1i}\,, \tag{17}$$

that is a system of $m$ linear equations with $m-1$ unknowns. By dropping the $i=1$ redundant equation, and denoting $\alpha_{ij} = Q_{j+1,i+1}$, $\beta_i = Q_{1,i+1}$ and $x_j = n'_{j+1}$ for $i,j = 1, m-1$, we write the matrix equation

$$\begin{pmatrix} \alpha_{11} & \alpha_{12} & \cdots & \alpha_{m-1,1} \\ \alpha_{21} & \alpha_{22} & \cdots & \alpha_{m-1,2} \\ \vdots & \vdots & \ddots & \vdots \\ \alpha_{m-1,1} & \alpha_{m-1,2} & \cdots & \alpha_{m-1,m-1} \end{pmatrix} \begin{pmatrix} x_1 \\ x_2 \\ \vdots \\ x_{m-1} \end{pmatrix} = \begin{pmatrix} \beta_1 \\ \beta_2 \\ \vdots \\ \beta_{m-1} \end{pmatrix} \tag{18}$$

that we solve with the Gauss-Jordan elimination method [8] to derive the atomic level population ratios $n'_j$. With $n_j/n = n'_j/(1+\sum_{k=2}^{m} n'_k))$, line intensities are finally obtained for each transition $j \rightarrow i$:

$$I_{ji} = \frac{h}{4\pi} N \frac{n'_j}{1+\sum_{k=2}^{m} n'_k} A_{ji} \nu_{ji} \ . \tag{19}$$

The high-resolution solar spectral irradiance $F_\lambda$ given in [6] and [7] at 1 au is converted into mean intensity in the coma using $J_{ij} = J(\nu_{ij}) = \frac{F_\lambda \lambda_{ij}^2}{4\pi c} r^{-2}$ where $r$ is in au. Relative abundances of atoms 1 and 2 can then be obtained using

$$\log \frac{N_1}{N_2} = \log \frac{I_{\rm obs,1}}{I_{\rm mod,1}} - \log \frac{I_{\rm obs,2}}{I_{\rm mod,2}} \ , \tag{20}$$

where $I_{\rm obs}$ and $I_{\rm mod}$ ($= I_{ji}$ for $N = 1$ cm$^{-2}$) are the observed and computed line intensities integrated over the observed line profile, respectively. The ratios $\log(I_{\rm obs,i}/I_{\rm mod,i})$ are computed for each observed line of a given atom, and then averaged to derive the abundance ratio.

In Fig. 6, the FeI lines intensities computed with the model, $I_{\rm mod}$, are compared to the measured intensities, $I_{\rm obs}$, for four comets. There is an overall agreement between the observed and computed spectra with some dispersion due to measurement errors and uncertainties on atomic data. The $I_{\rm obs}/I_{\rm mod}$ ratios are shown in Fig. 4 on a log scale for both the FeI and NiI lines. Although the dispersion of $\log(I_{\rm obs}/I_{\rm mod})$ for individual lines can be high due to other unknown blends or to model inaccuracies (Section 4.1.3), differences between comets are immediately seen. In Table 2 we give the Ni/Fe abundance ratio computed with the multilevel model for all comets of our sample.

For comets 103P and especially C/2016 R2, the dispersion of the intensity ratios is higher than for Ikeya-Seki, and some bright lines not well reproduced. In Sect. 4.1.3, we explore some possibilities to better reproduce the observed intensities but with no real improvement (and in any case no effect on the abundance ratios). Differences between Ikeya-Seki and other comets with respect to the model

could be, at least in part, attributed to the strong difference in heliocentric velocities, +110 km $s^{-1}$ for Ikeya-Seki versus +3.5, -5.6 and +25.6 km $s^{-1}$ for 103P, C/2016 R2 and C/2002 T7, respectively. The solar spectrum shows deep FeI and NiI absorption lines so that the radiation reaching the comet is strongly dimmed at low heliocentric velocities (Fig. 7). For high enough Doppler velocities, the radiation reaching the comet is expected to be more homogeneous for the different metallic lines, and closer to a blackbody.

#### 4.1.3 Tests, robustness and possible improvements

We modified the constraints on the selected energy levels and minimum transition strength, considering up to 668 energy levels and 3435 transitions for FeI. No significant changes of the level populations and line intensities can be observed in the spectral range of interest, i.e., 3300-4500 Å. We also considered alternative atomic data sets, in particular from [9], and found no significant differences in the model results.

The effect of collisions was also investigated, to try to better fit the observed line intensities. A collisional term $C_{ij}$ was added to the $Q_{ij}$ defined in Sect. 4.1.2, with $C_{ij}/C_{ji} = (g_j/g_i) \times 10^{\theta(\chi_i - \chi_j)}$. An approximate formula for estimating collisions with electrons is given by [10]. Given the low density and low temperature prevailing in cometary comae, collisions with electrons are negligible. Collisions with atoms or molecules might be considered but, as far as we know, no estimates are available for cometary atmospheres. We thus parametrized collisional de-excitation as $C_{ji} = \epsilon\,[\theta(\chi_j - \chi_i)]^{\delta}$ where $\epsilon$ and $\delta$ are free parameters. Tests done by varying these parameters indicate that introducing collisions does not improve the modeling, and most often gives worse fits.

We also considered extinction by dust in the inner coma using the standard CCM extinction curve [11]. Both the incoming solar radiation and the outward emitted lines are assumed to be reddened. For C/2016 R2, assuming $A_V \simeq 1.5$ (which is a reasonable value for the extinction in the inner coma [12]) makes dispersion in Fig. 5 slightly smaller (while the abundance ratio is unchanged).

Finally one should keep in mind that the fit of individual lines might be affected by the lower spectral resolution of the solar spectrum at wavelengths smaller than 2960 Å. Several transitions from the ground level do occur in that wavelength range for which the incoming solar flux might not be accurately estimated, at least at low heliocentric velocities.

#### 4.1.4 Multilevel versus three-level model

The comparison of the two models (Extended data Fig. 7) shows that the 3-level atomic populations reproduce fairly well the populations computed with the multilevel model and the Kurucz solar spectrum, provided that the blackbody temperature used in the 3-level model is significantly lower than the Sun effective temperature. We also estimated the excitation temperature using the FeI line intensities generated by the multilevel model, following Eq. 14. For cometary heliocentric velocities of 5 km $s^{-1}$ and 100 km $s^{-1}$, we derive $T \simeq 4000$ K and $T \simeq 4500$ K, respectively. The fact that the excitation temperature is smaller than the effective temperature of the Sun (5800 K) is thus mostly due to the fact that the flux from the solar spectrum is fainter than a blackbody due to the numerous absorption lines, in particular when the Doppler velocity is close to zero (Extended data Fig. 7).

The overall agreement between the Ni/Fe abundances estimated with the two models is good but (Extended data Fig. 7) but there is a clear systematic offset: the abundance ratios derived with the 3-level model are 0.2 dex higher than the abundance ratios derived with the multilevel model. A better agreement is obtained by assuming $T(\mathrm{NiI}) = T(\mathrm{FeI})+180$ K in the 3-level model.

## 4.2 Iron and nickel carbonyls

Following [13, 14], we estimate the condensation / sublimation temperature $T_s$ of these substances by solving the equation

$$f_x \, n \, k \, T_s = P_{v,x}(T_s) \tag{21}$$

where $f_x$ the relative abundance of species $x$, $n$ is the number density of the gas, $k$ the Boltzmann constant, and $P_{v,x}$ the vapor pressure given by the relation

$$\log_{10} P_{v,x}(T) = -A/T \, + \, B \, . \tag{22}$$

The constant $A$ and $B$ for $Fe(CO)_5$ and $Ni(CO)_4$ are obtained from [15, 16], that is $A = 2097$ K and $B = 11.62$ for $Fe(CO)_5$, $A = 1534$ K and $B = 10.87$ for $Ni(CO)_4$, with $P_{v,x}$ in dyn cm$^{-2}$. We consider relative abundances $f_x$ between $10^{-3}$ and $10^{-5} \times f_x(H_2O)$, for both $Fe(CO)_5$ and $Ni(CO)_4$, and we adopt $n = 10^{13}$ cm$^{-3}$ as [14]. The resulting sublimation temperatures of the iron and nickel carbonyls (respectively 97-108 K and 74-82K) are intermediate between the sublimation temperatures of $H_2O$ and $CO_2$ (152 and 72 K). CO sublimates at 25 K.

The sublimation rate (in molecules cm$^{-2}$ s$^{-1}$) from the surface of pure ice into vaccum can be expressed as [17]:

$$Z_x(T) = \frac{P_{v,x}(T)}{\sqrt{2\pi m_x k T}} \tag{23}$$

where $T$ is the ice temperature and $m_x$ the mass of the species $x$. Sublimation rates of $Fe(CO)_5$ and $Ni(CO)_4$ are shown in Fig. 3. They are intermediate between those of $H_2O$ and $CO_2$. Interestingly, the sublimation rate of $Ni(CO)_4$ is significantly higher than the sublimation rate of $Fe(CO)_5$, as illustrated on the right panel of Fig. 3.

# References


[1]G. W. Preston, "The spectrum of Ikeya-Seki (1965f)", ApJ **147**, 718–742 (1967).

[2]C. Arpigny, "On the nature of comets.", in Proceedings of the robert a. welch foundation conferences on chemical research xxi, cosmochemistry, edited by W. Mulligan (1978), p. 9.

[3]C. Arpigny, "Relative abundances of the heavy elements in comet Ikeya-Seki /1965 VIII/", in Liege international astrophysical colloquia, Vol. 22, edited by A. Boury, N. Grevesse, and L. Remy-Battiau, Liege International Astrophysical Colloquia (Jan. 1979), pp. 189–197.

[4]P. A. M. van Hoof, "Recent Development of the Atomic Line List", Galaxies **6**, 63 (2018).

[5]C. E. Moore, *Partial Grotriam diagrams of astrophysical interest* (1968).

[6]R. L. Kurucz, I. Furenlid, J. Brault, and L. Testerman, *Solar flux atlas from 296 to 1300 nm* (1984).

[7]L. A. Hall and G. P. Anderson, "High-resolution solar spectrum between 2000 and 3100 Å.", J. Geophys. Res. **96**, 12, 927–12, 931 (1991).

[8]W. H. Press, S. A. Teukolsky, W. T. Vetterling, and B. P. Flannery, *Numerical recipes in FORTRAN. The art of scientific computing* (1992).

[9]G. Nave, S. Johansson, R. C. M. Learner, A. P. Thorne, and J. W. Brault, "A New Multiplet Table for Fe i", ApJS **94**, 221 (1994).

[10]H. van Regemorter, "Rate of Collisional Excitation in Stellar Atmospheres.", ApJ **136**, 906 (1962).

[11]J. A. Cardelli, G. C. Clayton, and J. S. Mathis, "The Relationship between Infrared, Optical, and Ultraviolet Extinction", ApJ **345**, 245 (1989).

[12]P. Lacerda and D. Jewitt, "Extinction in the Coma of Comet 17P/Holmes", ApJ **760**, L2, L2 (2012).

[13]T. Yamamoto, N. Nakagawa, and Y. Fukui, "The chemical composition and thermal history of the ice of a cometary nucleus", A&A **122**, 171–176 (1983).

[14]T. Yamamoto, "Formation environment of cometary nuclei in the primordial solar nebula", A&A **142**, 31–36 (1985).

[15]A. G. Gilbert and K. G. P. Sulzmann, "The Vapor Pressure of Iron Pentacarbonyl", Journal of the Electrochemical Society **121**, 832 (1974).

[16]D. R. Stull, "Vapor Pressure of Pure Substances. Organic and Inorganic Compounds", Ind. Eng. Chem. **39**, 517 (1947).

[17]A. H. Delsemme, "Chemical composition of cometary nuclei", in Iau colloq. 61: comet discoveries, statistics, and observational selection, edited by L. L. Wilkening (Jan. 1982), pp. 85–130.

[18]H. F. Levison, "Comet Taxonomy", in Completing the inventory of the solar system, Vol. 107, edited by T. Rettig and J. M. Hahn, Astronomical Society of the Pacific Conference Series (Jan. 1996), pp. 173–191.

[19]H. Weaver, P. Feldman, M. A'Hearn, N. Dello Russo, and A. Stern, "Comet 103P/Hartley", IAU Circ. **9183**, 1 (2010).

[20]N. X. Roth, E. L. Gibb, B. P. Bonev, M. A. DiSanti, N. Dello Russo, A. J. McKay, J. Vervack Ronald J., H. Kawakita, M. Saki, N. Biver, D. Bockelée-Morvan, L. M. Feaga, N. Fougere, A. L. Cochran, M. Combi, and Y. Shou, "Probing the Evolutionary History of Comets: An Investigation of the Hypervolatiles CO, $CH_4$, and $C_2H_6$ in the Jupiter-family Comet 21P/Giacobini-Zinner", AJ **159**, 42, 42 (2020).

[21]M. A. DiSanti, W. M. Anderson, G. L. Villanueva, B. P. Bonev, K. Magee-Sauer, E. L. Gibb, and M. J. Mumma, "Depleted Carbon Monoxide in Fragment C of the Jupiter-Family Comet 73P/Schwassmann-Wachmann 3", ApJ **661**, L101–L104 (2007).

[22]H. Böhnhardt, M. J. Mumma, G. L. Villanueva, M. A. DiSanti, B. P. Bonev, M. Lippi, and H. U. Käufl, "The Unusual Volatile Composition of the Halley-Type Comet 8P/Tuttle: Addressing the Existence of an Inner Oort Cloud", ApJ **683**, L71 (2008).

[23]R. E. Lupu, P. D. Feldman, H. A. Weaver, and G.-P. Tozzi, "The Fourth Positive System of Carbon Monoxide in the Hubble Space Telescope Spectra of Comets", ApJ **670**, 1473–1484 (2007).

[24]M. A. DiSanti, B. P. Bonev, K. Magee-Sauer, N. Dello Russo, M. J. Mumma, D. C. Reuter, and G. L. Villanueva, "Detection of Formaldehyde Emission in Comet C/2002 T7 (LINEAR) at Infrared Wavelengths: Line-by-Line Validation of Modeled Fluorescent Intensities", ApJ **650**, 470–483 (2006).

[25]L. Paganini, M. J. Mumma, G. L. Villanueva, M. A. DiSanti, B. P. Bonev, M. Lippi, and H. Boehnhardt, "Observations of Comet C/2009 P1 (Garradd) at 2.4 and 2.0 AU Before Perihelion", in Asteroids, comets, meteors 2012, Vol. 1667 (May 2012), p. 6331.

[26]L. Paganini, M. A. DiSanti, M. J. Mumma, G. L. Villanueva, B. P. Bonev, J. V. Keane, E. L. Gibb, H. Boehnhardt, and K. J. Meech, "The Unexpectedly Bright Comet C/2012 F6 (Lemmon) Unveiled at Near-infrared Wavelengths", AJ **147**, 15, 15 (2014).

509 [27]N. Biver, D. Bockelée-Morvan, G. Paubert, R. Moreno, J. Crovisier, J. Boissier, E. Bertrand, H.
510 Boussier, F. Kugel, A. McKay, N. Dello Russo, and M. A. DiSanti, "The extraordinary composition
511 of the blue comet C/2016 R2 (PanSTARRS)", A&A **619**, A127, A127 (2018).

512 [28]K. Wierzchos and M. Womack, "C/2016 R2 (PANSTARRS): A Comet Rich in CO and Depleted in
513 HCN", AJ **156**, 34, 34 (2018).

514 [29]S. Faggi, M. J. Mumma, G. L. Villanueva, L. Paganini, and M. Lippi, "Quantifying the Evolution of
515 Molecular Production Rates of Comet 21P/Giacobini-Zinner with iSHELL/NASA-IRTF", AJ **158**,
516 254, 254 (2019).

517 [30]M. de Val-Borro, M. Küppers, P. Hartogh, L. Rezac, N. Biver, D. Bockelée-Morvan, J. Crovisier, C.
518 Jarchow, and G. L. Villanueva, "A survey of volatile species in Oort cloud comets C/2001 Q4 (NEAT)
519 and C/2002 T7 (LINEAR) at millimeter wavelengths", A&A **559**, A48, A48 (2013).

# 5 Extended data

Table 1: **Circumstances of UVES spectra**.
Comets observed with the UVES spectrograph at the ESO VLT with their dynamical classes and observing circumstances. In several cases, $N$ spectra have been averaged. $r$ and $\Delta$ are the heliocentric and geocentric distances in au and $\dot{r}$ and $\dot{\Delta}$ their respective velocities in km/s. The offset $d$ from the nucleus, the slit width $w$ and the slit height $h$ are given in arc seconds. Type refers to their dynamical class [18] : HFC (Halley Family) and JFC (Jupiter Family) correspond to ecliptic comets with short periods ($< 200$ years), EXT corresponds to external comets with semi-major axis $a < 10000$ au and NEW corresponds to external comets which directly come from the Oort cloud ($a > 10000$ au).

| | Comet | Type | Dates | $\lambda$ range | $N$ | $r$ | $\dot{r}$ | $\Delta$ | $\dot{\Delta}$ | $d$ | $w$ | $h$ |
|---|---|---|---|---|---|---|---|---|---|---|---|---|
| 1 | 103P/Hartley 2 | JFC | 2010-11-05:2010-11-10 | 3105-3910 | 4 | 1.07 | 3.5 | 0.17 | 7.5 | 0 | 0.44 | 9.5 |
| 2 | | JFC | 2010-11-11 | 3105-3910 | 1 | 1.08 | 4.4 | 0.19 | 8.2 | 10 | 0.44 | 9.5 |
| 3 | | JFC | 2010-11-11 | 3105-3910 | 1 | 1.08 | 4.4 | 0.19 | 8.2 | 20 | 0.44 | 9.5 |
| 4 | | JFC | 2010-11-11 | 3105-3910 | 1 | 1.08 | 4.4 | 0.19 | 8.2 | 30 | 0.44 | 9.5 |
| 5 | 21P/Giacobini-Zinner | JFC | 2018-09-18 | 3104-3879 | 1 | 1.02 | 2.9 | 0.40 | 4.2 | 0 | 0.44 | 9.5 |
| 6 | 73P/Schwassmann-Wachmann 3 | JFC | 2006-05-27 | 3104-3911 | 1 | 0.95 | -4.2 | 0.15 | 12.3 | 0 | 0.60 | 9.5 |
| 7 | 88P/Howell | JFC | 2004-04-18:2004-05-24 | 3286-4513 | 11 | 1.40 | 3.0 | 1.65 | -3.4 | 0 | 0.44 | 7.5 |
| 8 | 8P/Tuttle | HFC | 2008-01-16:2008-02-04 | 3105-3911 | 3 | 1.03 | 0.0 | 0.50 | 23.0 | 0 | 0.44 | 9.5 |
| 9 | 9P/Tempel 1 | JFC | 2005-06-02:2005-07-11 | 3104-3879 | 13 | 1.50 | 0.0 | 0.85 | 7.0 | 0 | 0.44 | 9.5 |
| 10 | C/2000 WM1 (LINEAR) | NEW | 2002-03-07:2002-03-08 | 3286-4513 | 4 | 1.10 | 28.3 | 1.24 | 0.2 | 10 | 0.45 | 7.5 |
| 11 | | NEW | 2002-03-22:2002-03-23 | 3286-4513 | 4 | 1.33 | 27.9 | 1.24 | -0.2 | 2 | 0.45 | 7.5 |
| 12 | C/2001 Q4 (NEAT) | NEW | 2004-05-05 | 3286-4513 | 1 | 0.98 | -5.4 | 0.32 | -4.1 | 3 | 0.44 | 9.5 |
| 13 | | NEW | 2004-05-06 | 3286-4513 | 1 | 0.98 | -5.4 | 0.32 | -3.3 | 13 | 0.44 | 7.5 |
| 14 | | NEW | 2004-05-06 | 3286-4513 | 1 | 0.97 | -4.9 | 0.32 | 1.9 | 200 | 0.44 | 7.5 |
| 15 | | NEW | 2004-05-07 | 3286-4513 | 1 | 0.97 | -4.8 | 0.32 | 2.2 | 0 | 0.44 | 9.5 |
| 16 | C/2002 T7 (LINEAR) | NEW | 2004-05-06 | 3736-4994 | 1 | 0.68 | 15.8 | 0.61 | -65.6 | 5 | 0.44 | 9.5 |
| 17 | | NEW | 2004-05-06 | 3105-3878 | 1 | 0.68 | 15.8 | 0.61 | -65.6 | 5 | 0.44 | 9.5 |
| 18 | | NEW | 2004-05-25 | 3736-4994 | 1 | 0.93 | 25.4 | 0.38 | 51.9 | 0 | 0.44 | 9.5 |
| 19 | | NEW | 2004-05-26 | 3104-3878 | 1 | 0.94 | 25.6 | 0.41 | 55.0 | 0 | 0.40 | 9.5 |
| 20 | | NEW | 2004-05-27 | 3104-3878 | 1 | 0.94 | 25.6 | 0.42 | 55.2 | 0 | 0.40 | 9.5 |
| 21 | C/2002 V1 (NEAT) | NEW | 2003-01-08:2003-01-10 | 3286-4513 | 4 | 1.20 | -37.0 | 0.84 | 8.0 | 0 | 0.45 | 7.5 |
| 22 | | NEW | 2003-03-21 | 3286-4513 | 1 | 1.01 | 39.8 | 1.63 | 42.0 | 0 | 0.45 | 7.5 |
| 23 | C/2002 X5 (Kudo-Fujikawa) | EXT | 2003-02-19 | 3286-4513 | 1 | 0.70 | 43.0 | 0.86 | -5.0 | 0 | 0.45 | 7.5 |
| 24 | | EXT | 2003-03-07 | 3286-4513 | 3 | 1.06 | 37.0 | 0.99 | 29.4 | 3 | 0.45 | 7.5 |
| 25 | C/2002 Y1 (Juels-Holvorcem) | EXT | 2003-05-29:2003-05-30 | 3286-4513 | 4 | 1.15 | 24.1 | 1.55 | -7.2 | 2 | 0.40 | 7.5 |
| 26 | C/2003 K4 (LINEAR) | NEW | 2004-05-04 | 3104-3879 | 1 | 1.20 | 14.8 | 1.51 | -28.2 | 0 | 0.44 | 9.5 |
| 27 | C/2009 P1 (Garradd) | NEW | 2011-05-11 | 3105-3911 | 1 | 3.25 | -16.9 | 3.50 | -44.7 | 0 | 0.44 | 9.5 |
| 28 | | NEW | 2011-06-15 | 3105-3911 | 1 | 2.90 | -16.9 | 2.57 | -46.4 | 0 | 0.44 | 9.5 |
| 29 | | NEW | 2011-07-25 | 3105-3885 | 1 | 2.52 | -16.5 | 1.64 | -29.3 | 0 | 0.44 | 9.5 |
| 30 | | NEW | 2011-09-10:2011-09-12 | 3044-3916 | 3 | 2.08 | -14.8 | 1.48 | 15.1 | 0 | 0.44 | 9.5 |
| 31 | C/2012 F6 (Lemmon) | EXT | 2013-02-02 | 3104-3911 | 3 | 1.20 | -24.0 | 0.99 | -4.5 | 0 | 0.44 | 9.5 |
| 32 | C/2015 ER61 | EXT | 2017-04-13:2017-04-15 | 3104-3879 | 2 | 2.04 | 6.8 | 1.94 | -2.0 | 0 | 0.44 | 9.5 |
| 33 | C/2016 R2 (PANSTARRS) | EXT | 2018-02-14 | 3286-4557 | 3 | 2.75 | -5.9 | 2.43 | 20.1 | 0 | 0.44 | 7.5 |
| 34 | | EXT | 2018-02-16 | 3737-4994 | 2 | 2.75 | -5.8 | 2.46 | 20.2 | 0 | 0.44 | 7.5 |

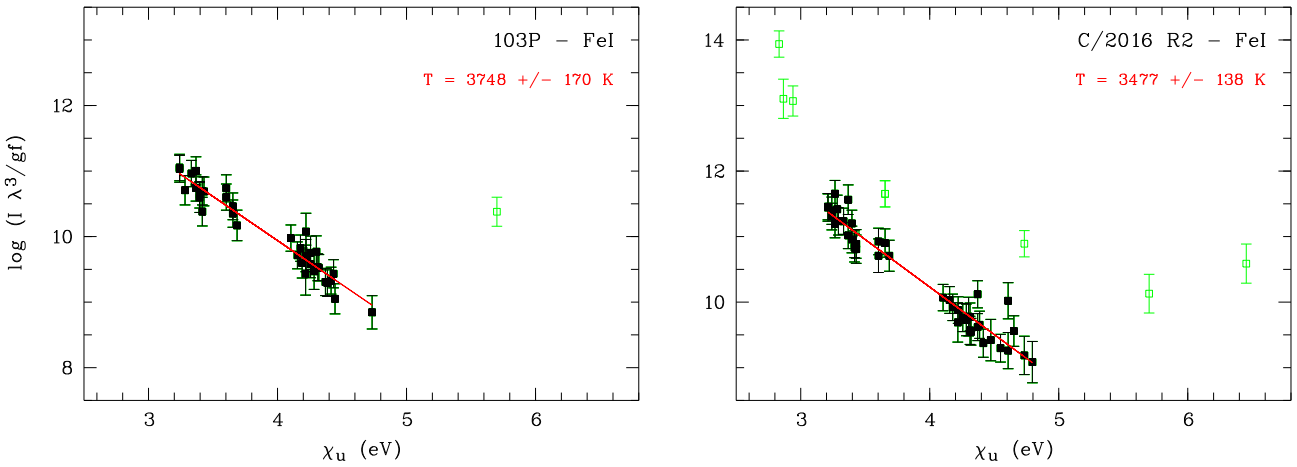


Figure 4: **Empirical determination of the excitation temperature.** FeI emission lines observed in two representative comets are used. Outliers not considered in the fit are shown in green. For C/2016 R2 (and only for that comet) additional outliers were discarded through an iterative fit. Error bars account for the errors on the measured intensities and an uncertainty of $\log(gf)$ assumed to be 0.2 dex.

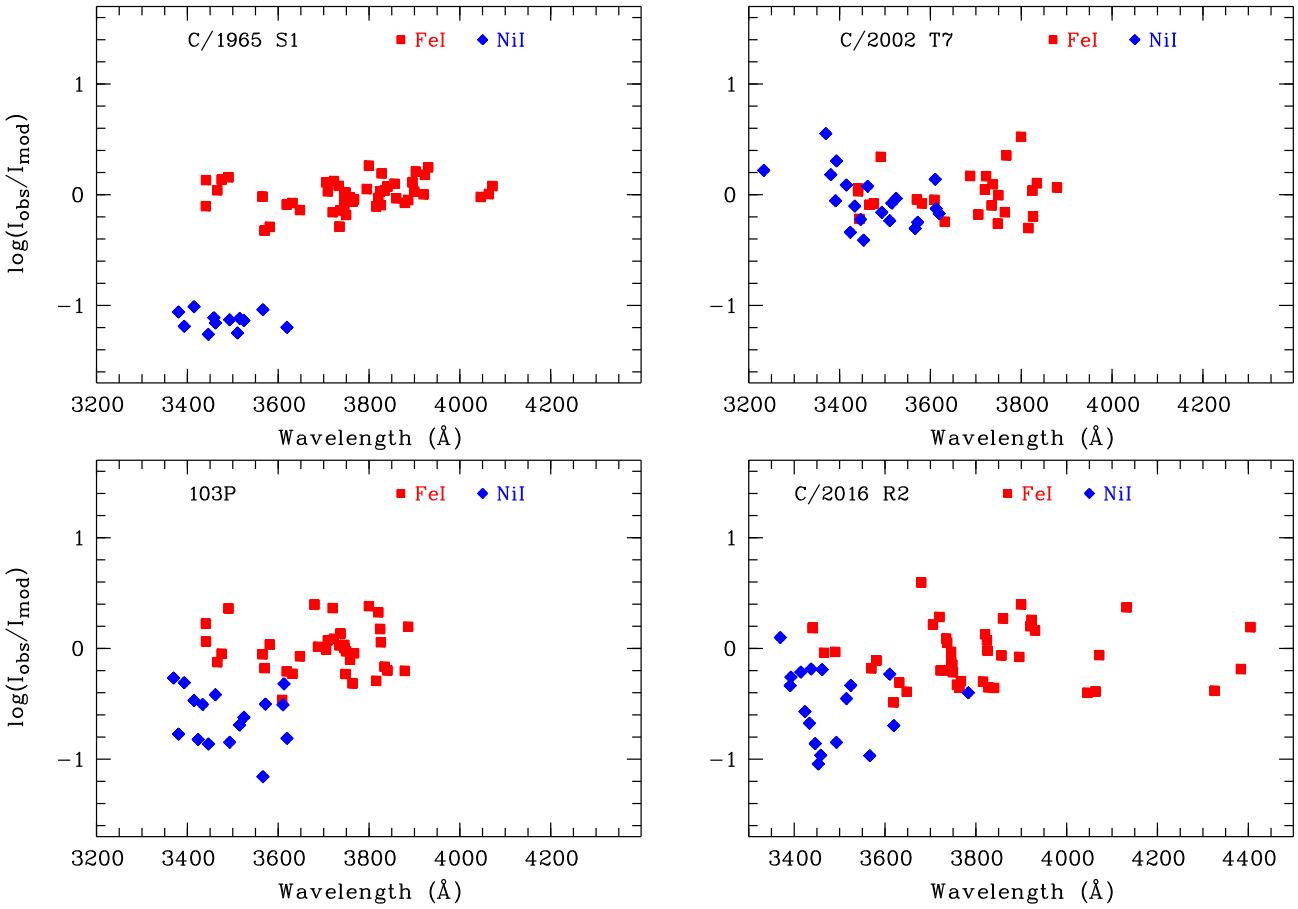


Figure 5: **Abundance ratio determination.** The ratio $\log(I_{\rm obs}/I_{\rm mod})$ for the FeI (red) and NiI (blue) lines measured in four comets. The ratios have been shifted on the y-axis so that the mean of $\log(I_{\rm obs}/I_{\rm mod})$ is zero for FeI. The few outliers have been discarded. The difference of the means computed for FeI and NiI gives the log(Ni/Fe) abundance ratio (cf. Eq. 20).

Table 2: The Ni/Fe abundance ratios derived from the 3-level model(*) and from the multilevel model(**). The column densities $N$ (atoms/cm$^2$) and the production rates $Q$ (atoms/s) come from the multilevel model.

| | | | 3-level model | | multi-level model | | | | |
|---|---|---|---|---|---|---|---|---|---|
| ID | Comet | $n_{lines}$ (FeI / NiI) | T(K) | log(Ni/Fe)* | log($N_{col}$[FeI]) | log($N_{col}$[NiI]) | log($Q$[FeI]) | log($Q$[NiI]) | log(NiI/FeI)** |
| 1 | 103P | 36 / 16 | 3748 ± 170 | -0.47 ± 0.09 | 8.84 ± 0.04 | 8.22 ± 0.06 | 21.55 ± 0.04 | 20.93 ± 0.06 | -0.62 ± 0.07 |
| 2 | | 16 / 7 | 3290 ± 180 | -0.47 ± 0.08 | 8.33 ± 0.05 | 7.65 ± 0.06 | 21.98 ± 0.05 | 21.30 ± 0.06 | -0.68 ± 0.08 |
| 3 | | 10 / 2 | 4791 ± 1278 | -0.27 ± 0.27 | 8.05 ± 0.12 | 7.53 ± 0.21 | 22.01 ± 0.12 | 21.48 ± 0.21 | -0.52 ± 0.24 |
| 4 | | 6 / 2 | 3267 ± 934 | -0.08 ± 0.28 | 7.85 ± 0.18 | 7.51 ± 0.21 | 21.98 ± 0.18 | 21.64 ± 0.21 | -0.34 ± 0.28 |
| 5 | 21P | 8 / 23 | 3017 ± 590 | 0.63 ± 0.16 | 8.74 ± 0.14 | 9.20 ± 0.07 | 21.85 ± 0.14 | 22.30 ± 0.07 | 0.46 ± 0.16 |
| 6 | 73P | 6 / 15 | 2785 ± 1185 | 0.98 ± 0.28 | 8.54 ± 0.21 | 9.14 ± 0.09 | 21.23 ± 0.21 | 21.83 ± 0.09 | 0.60 ± 0.23 |
| 7 | 88P | 21 / 13 | 4212 ± 782 | 0.01 ± 0.18 | 8.61 ± 0.09 | 8.43 ± 0.11 | 21.78 ± 0.09 | 21.60 ± 0.11 | -0.18 ± 0.14 |
| 8 | 8P | 9 / 10 | 3815 ± 1164 | -0.07 ± 0.22 | 8.68 ± 0.14 | 8.62 ± 0.14 | 21.87 ± 0.14 | 21.81 ± 0.14 | -0.06 ± 0.20 |
| 9 | 9P | 5 / 1 | 3748 ± 554 | 0.30 ± 0.33 | 7.37 ± 0.12 | 7.73 ± 0.30 | 20.72 ± 0.12 | 21.07 ± 0.30 | 0.36 ± 0.32 |
| 10 | C/2000 WM1 | 14 / 7 | 4636 ± 463 | -0.06 ± 0.14 | 8.17 ± 0.06 | 7.82 ± 0.06 | 22.63 ± 0.06 | 22.28 ± 0.06 | -0.35 ± 0.08 |
| 11 | | 13 / 8 | 4272 ± 537 | 0.11 ± 0.14 | 8.27 ± 0.07 | 8.07 ± 0.07 | 22.12 ± 0.07 | 21.92 ± 0.07 | -0.20 ± 0.10 |
| 12 | C/2001 Q4 | 13 / 10 | 4213 ± 530 | 0.27 ± 0.14 | 9.70 ± 0.07 | 9.72 ± 0.11 | 23.18 ± 0.07 | 23.20 ± 0.11 | 0.03 ± 0.13 |
| 13 | | 8 / 8 | 3519 ± 589 | 0.15 ± 0.19 | 9.07 ± 0.12 | 9.07 ± 0.12 | 23.09 ± 0.12 | 23.08 ± 0.12 | -0.01 ± 0.17 |
| 14 | | 7 / 4 | 5069 ± 866 | 0.33 ± 0.23 | 7.76 ± 0.07 | 7.85 ± 0.18 | 22.96 ± 0.07 | 23.05 ± 0.18 | 0.08 ± 0.19 |
| 15 | | 17 / 13 | 3481 ± 320 | 0.13 ± 0.12 | 9.27 ± 0.07 | 9.25 ± 0.07 | 22.29 ± 0.07 | 22.26 ± 0.07 | -0.03 ± 0.10 |
| 16 | C/2002 T7 | 2 / 2 | 4000 ± 1000 | 0.20 ± 0.35 | 9.68 ± 0.21 | 9.49 ± 0.21 | 23.68 ± 0.21 | 23.49 ± 0.21 | -0.19 ± 0.30 |
| 17 | C/2002 T7 | 17 / 20 | 3570 ± 452 | 0.12 ± 0.13 | 9.25 ± 0.07 | 9.07 ± 0.07 | 23.25 ± 0.07 | 23.08 ± 0.07 | -0.17 ± 0.10 |
| 18 | | 18 / 2 | 3400 ± 326 | 0.56 ± 0.24 | 9.22 ± 0.08 | 9.43 ± 0.21 | 22.32 ± 0.08 | 22.53 ± 0.21 | 0.21 ± 0.23 |
| 19 | | 26 / 21 | 4239 ± 385 | 0.16 ± 0.09 | 9.22 ± 0.04 | 9.16 ± 0.05 | 22.34 ± 0.04 | 22.29 ± 0.05 | -0.06 ± 0.07 |
| 20 | | 21 / 22 | 4059 ± 432 | 0.26 ± 0.10 | 9.16 ± 0.05 | 9.16 ± 0.06 | 22.29 ± 0.05 | 22.29 ± 0.06 | 0.00 ± 0.07 |
| 21 | C/2002 V1 | 23 / 15 | 4154 ± 419 | 0.08 ± 0.12 | 8.46 ± 0.05 | 8.33 ± 0.09 | 21.78 ± 0.05 | 21.64 ± 0.09 | -0.14 ± 0.10 |
| 22 | | 11 / 9 | 4250 ± 1776 | -0.01 ± 0.23 | 8.92 ± 0.13 | 8.92 ± 0.15 | 22.56 ± 0.13 | 22.56 ± 0.15 | 0.00 ± 0.20 |
| 23 | C/2002 X5 | 19 / 16 | 4115 ± 459 | 0.08 ± 0.13 | 8.49 ± 0.07 | 8.48 ± 0.09 | 21.94 ± 0.07 | 21.93 ± 0.09 | -0.01 ± 0.12 |
| 24 | | 10 / 12 | 4734 ± 713 | -0.20 ± 0.15 | 8.27 ± 0.08 | 7.90 ± 0.08 | 22.20 ± 0.08 | 21.83 ± 0.08 | -0.37 ± 0.11 |
| 25 | C/2002 Y1 | 15 / 11 | 3339 ± 335 | 0.04 ± 0.16 | 8.60 ± 0.05 | 8.49 ± 0.12 | 22.58 ± 0.05 | 22.47 ± 0.12 | -0.11 ± 0.13 |
| 26 | C/2003 K4 | 3 / 10 | 4000 ± 1000 | 0.24 ± 0.16 | 8.46 ± 0.09 | 8.23 ± 0.09 | 22.10 ± 0.09 | 21.87 ± 0.09 | -0.23 ± 0.13 |
| 27 | C/2009 P1 | 2 / 13 | 4000 ± 1000 | 0.85 ± 0.28 | 8.19 ± 0.21 | 8.61 ± 0.09 | 21.97 ± 0.21 | 22.39 ± 0.09 | 0.42 ± 0.23 |
| 28 | | 1 / 7 | 4000 ± 1000 | 0.47 ± 0.36 | 8.65 ± 0.30 | 8.68 ± 0.09 | 22.33 ± 0.30 | 22.37 ± 0.09 | 0.04 ± 0.31 |
| 29 | | 2 / 14 | 4000 ± 1000 | 0.69 ± 0.27 | 8.62 ± 0.21 | 9.05 ± 0.08 | 22.13 ± 0.21 | 22.57 ± 0.08 | 0.44 ± 0.23 |
| 30 | | 11 / 21 | 4131 ± 512 | 0.65 ± 0.10 | 8.77 ± 0.06 | 9.11 ± 0.05 | 22.28 ± 0.06 | 22.62 ± 0.05 | 0.34 ± 0.08 |
| 31 | C/2012 F6 | 27 / 23 | 4288 ± 340 | 0.13 ± 0.08 | 9.21 ± 0.03 | 9.07 ± 0.04 | 22.66 ± 0.03 | 22.52 ± 0.04 | -0.14 ± 0.05 |
| 32 | C/2015 ER61 | 19 / 15 | 3660 ± 452 | 0.07 ± 0.12 | 9.42 ± 0.07 | 9.24 ± 0.06 | 23.05 ± 0.07 | 22.87 ± 0.06 | -0.19 ± 0.09 |
| 33 | C/2016 R2 | 43 / 18 | 3477 ± 138 | -0.27 ± 0.09 | 9.87 ± 0.04 | 9.42 ± 0.08 | 23.46 ± 0.04 | 23.01 ± 0.08 | -0.45 ± 0.09 |
| 34 | | 25 / 1 | 3565 ± 219 | 0.04 ± 0.33 | 9.79 ± 0.06 | 9.73 ± 0.30 | 23.39 ± 0.06 | 23.33 ± 0.30 | -0.06 ± 0.31 |
| 35 | C/1965 S1 | 47 / 12 | 5136 ± 274 | -1.11 ± 0.09 | | | | | -1.14 ± 0.03 |

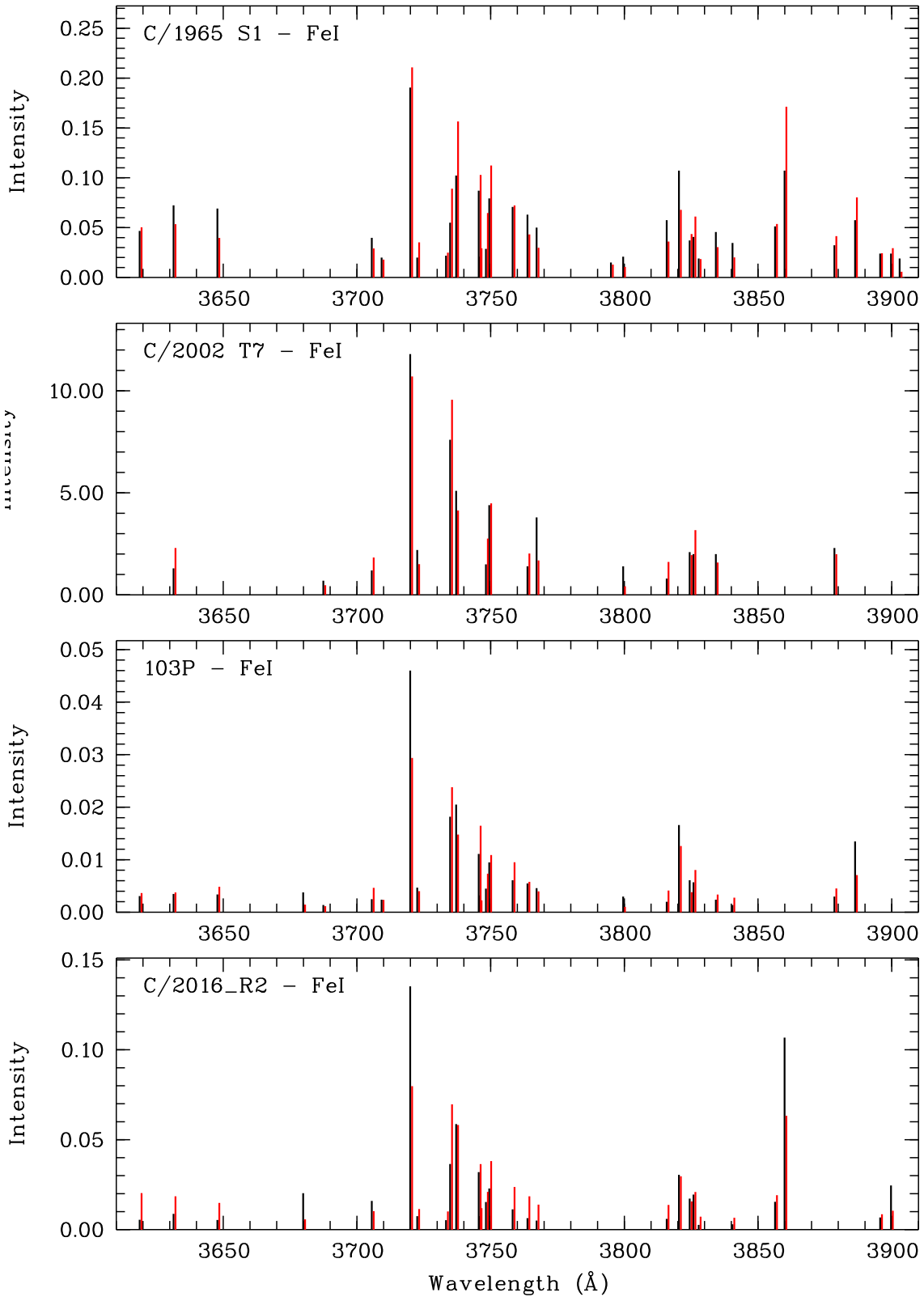


Figure 6: **Comparison of the observed and modeled spectra.** A portion of the FeI spectrum is shown for four representative comets. Observed lines are in black; computed lines are in red, shifted by 0.7 Å for visibility.

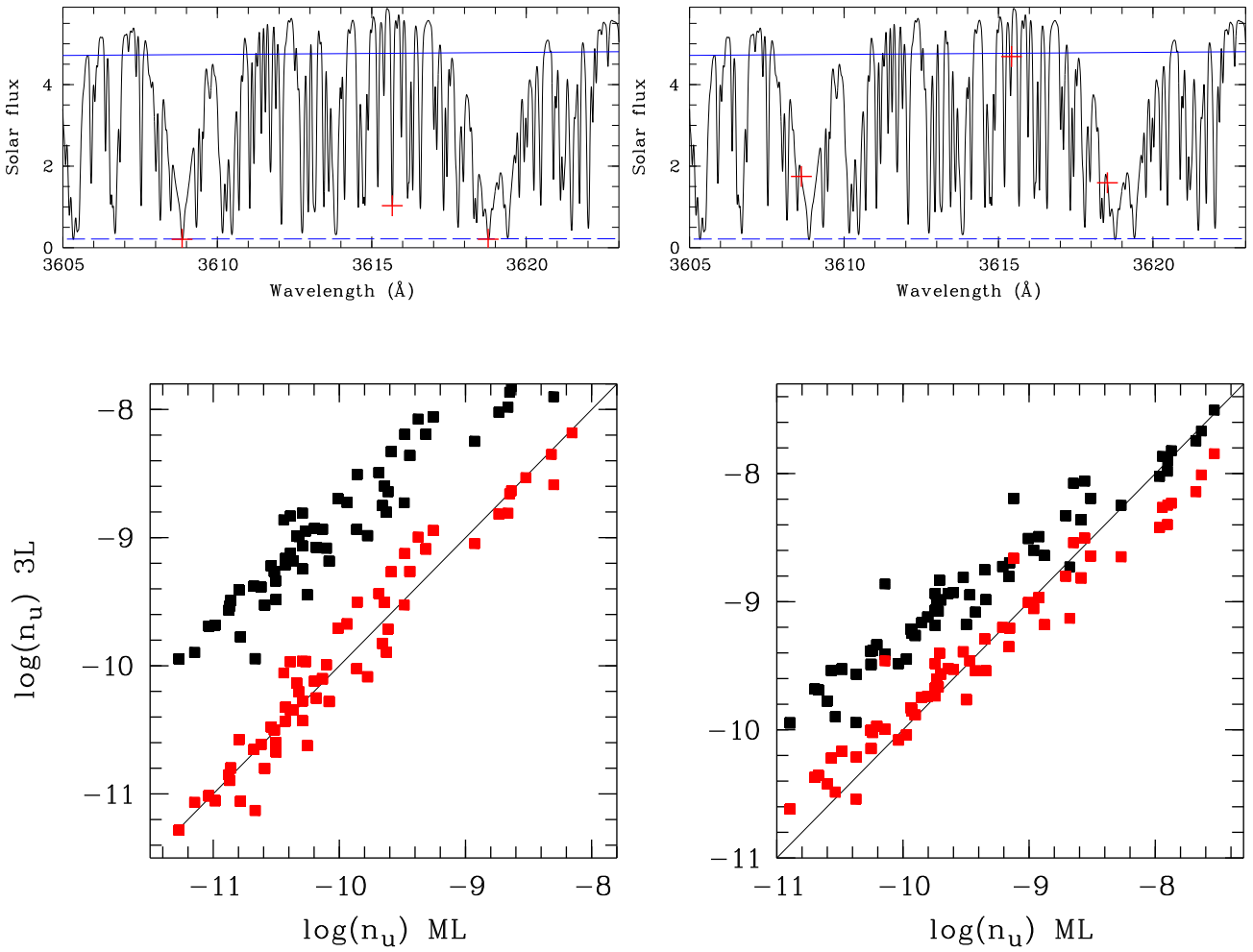


Figure 7: **Effect of the solar spectrum.**
Top: Sample of the Kurucz solar spectrum. The red crosses indicate the value of the solar flux involved in three cometary FeI transitions. The solid blue line represents a blackbody spectrum with $T = 5800\ K$, and the dashed blue line a blackbody spectrum with $T = 4000\ K$. Cometary heliocentric velocities are equal to 0 km $s^{-1}$ (left) and +20 km $s^{-1}$ (right). The solar flux is given in arbitrary units.
Bottom: Comparison of upper level populations computed for FeI with the 3-level and multilevel atomic models. *Left:* Black squares represent 3-level populations computed with a blackbody temperature of 5800 K (the color temperature of the Sun) while red squares represent 3-level populations computed with a temperature of 4400 K in better agreement with the mutilevel populations computed with the Kurucz solar spectrum . *Right:* Same as in the previous figure, but with the solar spectrum shifted by 20 km $s^{-1}$. The red squares represent 3-level populations computed with a temperature of 5000 K.

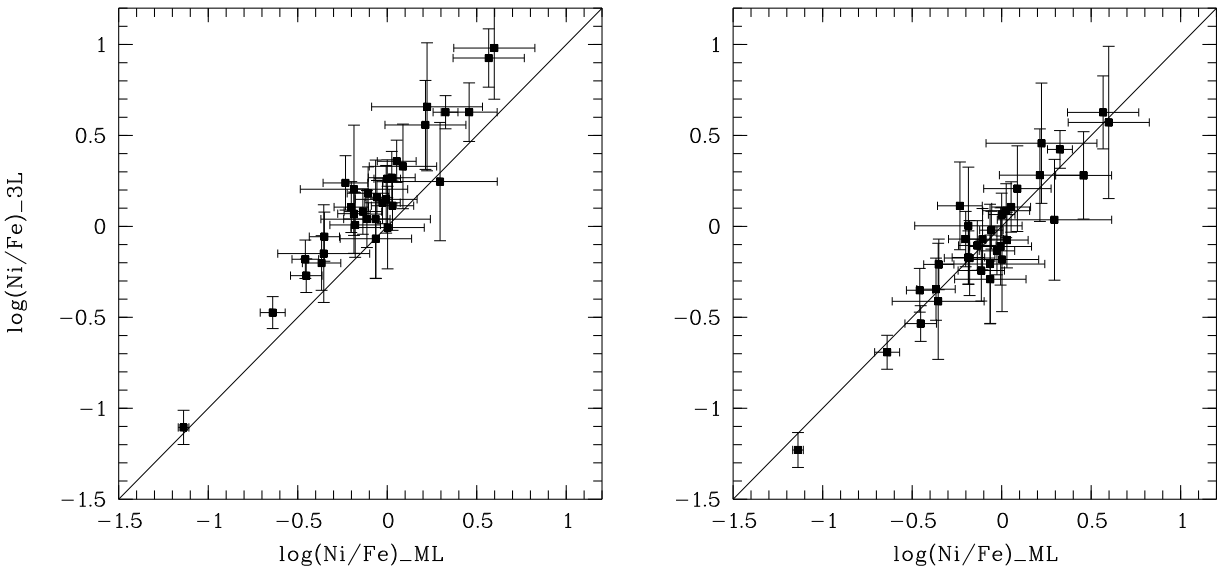


Figure 8: **Abundances from the two models.** Comparison of log(Ni/Fe) abundances derived with the multilevel (ML) model and the 3-level (3L) model for the comets of our sample. *Left:* Assuming $T$(NiI) = $T$(FeI). *Right:* With $T$(NiI) = $T$(FeI)+180 K.

Table 3: **Production rates of molecules and dust**. Logarithm of the production rates of the gaseous species $CO_2^+$, OH, CN (molecules/s) and logarithm of $Af\rho$ (in cm).

| | Comet | $CO_2^+$ | OH | CN | $Af\rho$ |
|---|---|---|---|---|---|
| 1 | 103P | 26.23±0.16 | 27.65±0.02 | 24.72±0.02 | 1.16±0.09 |
| 2 | | 26.25±0.33 | 27.74±0.05 | 24.77±0.03 | 1.65±0.11 |
| 3 | | 26.07±0.31 | 27.72±0.07 | 24.76±0.04 | 1.70±0.21 |
| 4 | | | 27.76±0.07 | 24.83±0.04 | 1.72±0.15 |
| 5 | 21P | 26.49±0.32 | 27.91±0.02 | 25.18±0.05 | 2.05±0.05 |
| 6 | 73P | | 27.85±0.01 | 25.30±0.04 | 1.26±0.06 |
| 7 | 88P | 26.87±0.12 | | 25.10±0.04 | 2.91±0.31 |
| 8 | 8P | | 27.90±0.01 | 25.28±0.03 | 2.19±0.13 |
| 9 | 9P | | 27.14±0.06 | 24.50±0.03 | 2.33±0.01 |
| 10 | C/2000 WM1 | 27.39±0.14 | | 25.81±0.03 | 3.81±0.06 |
| 11 | | 26.74±0.32 | | 25.47±0.03 | 3.31±0.07 |
| 12 | C/2001 Q4 | | | 26.01±0.02 | 3.36±0.06 |
| 13 | | 27.23±0.24 | | 26.14±0.03 | 3.36±0.04 |
| 14 | | | | 26.43±0.02 | 3.22±0.07 |
| 15 | | 27.35±0.20 | | 25.91±0.02 | 2.32±0.05 |
| 16 | C/2002 T7 | | | 26.55±0.02 | 3.55±0.04 |
| 17 | | 27.93±0.29 | 29.05±0.00 | 26.64±0.02 | 3.68±0.06 |
| 18 | | | | 25.88±0.04 | 2.52±0.05 |
| 19 | | 27.60±0.18 | 28.69±0.00 | 26.06±0.02 | 2.74±0.04 |
| 20 | | 27.51±0.24 | 28.65±0.01 | 26.02±0.02 | 2.71±0.04 |
| 21 | C/2002 V1 | 26.62±0.42 | | 25.34±0.02 | 2.52±0.21 |
| 22 | | | | 25.84±0.02 | 3.80±0.06 |
| 23 | C/2002 X5 | 27.36±0.14 | | 25.73±0.04 | 2.75±0.06 |
| 24 | | 27.11±0.12 | | 25.38±0.04 | 2.88±0.03 |
| 25 | C/2002 Y1 | 27.38±0.18 | | 25.84±0.02 | 3.71±0.03 |
| 26 | C/2003 K4 | | 28.55±0.01 | 25.83±0.02 | 3.68±0.07 |
| 27 | C/2009 P1 | | | 25.37±0.02 | 4.26±0.07 |
| 28 | | | 27.55±0.23 | 25.47±0.04 | 4.42±0.09 |
| 29 | | | 28.10±0.15 | 25.64±0.06 | 3.68±0.08 |
| 30 | | | 28.37±0.04 | 25.85±0.04 | 4.05±0.03 |
| 31 | C/2012 F6 | 27.37±0.39 | 28.90±0.01 | 26.16±0.09 | 3.62±0.11 |
| 32 | C/2015 ER61 | 27.05±0.42 | 29.31±0.01 | 26.31±0.06 | 4.39±0.02 |
| 33 | C/2016 R2 | 27.65±0.11 | 27.73±0.36 | 24.44±0.24 | 3.23±0.12 |
| 34 | | | 27.73±0.36 | 24.32±0.07 | 3.25±0.12 |

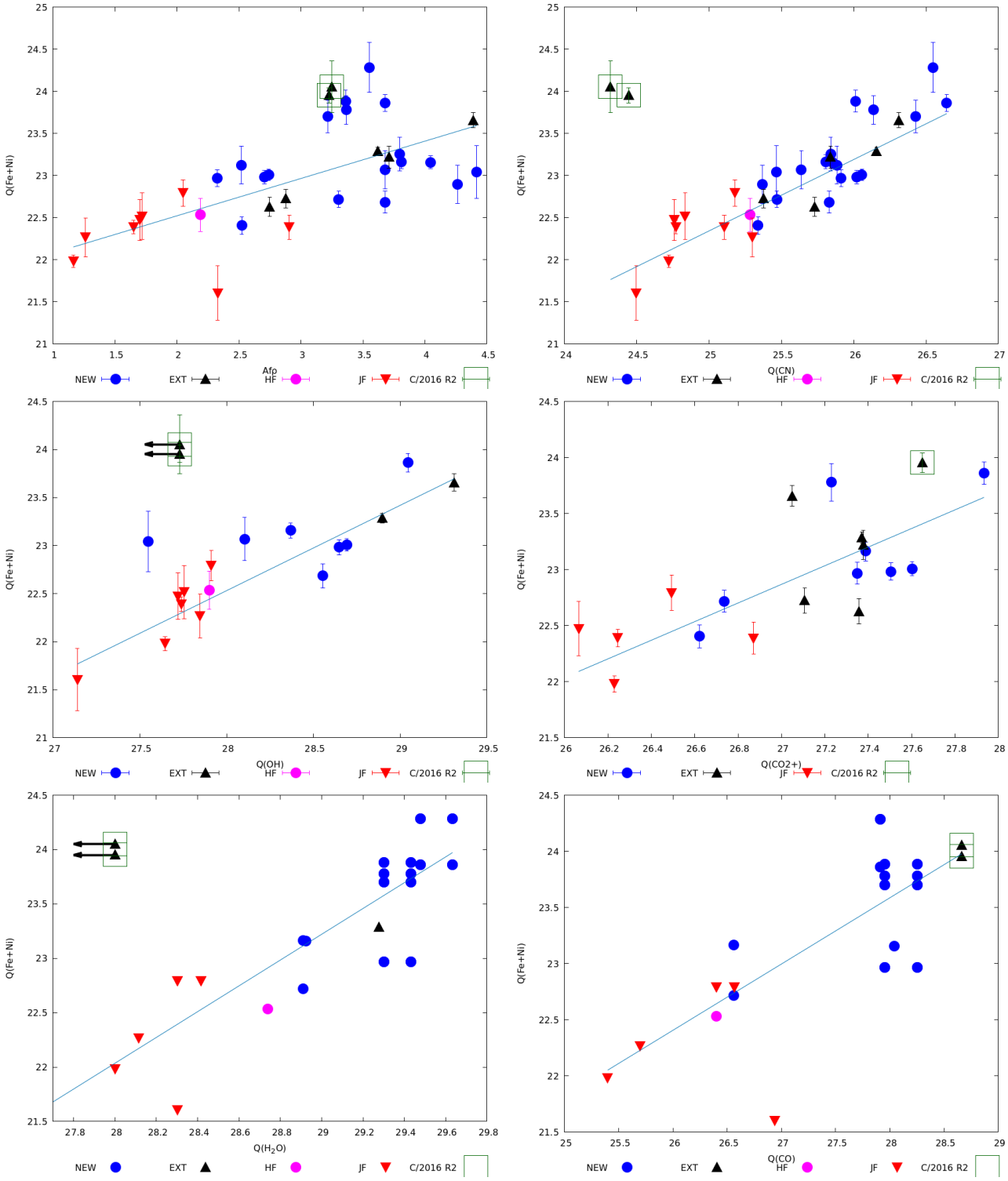


Figure 9: **Production rates correlations.** Comparison between the logarithm of various production rates. $Af\rho$ is a proxy for the dust production rate (see text). The various cometary types are color coded according to their dynamical classification (see 1) : Halley Family, Jupiter Family, external and new comets. The OH and $H_2O$ values relative to comet C/2016 R2 are upper limits. The production rates of $H_2O$ and CO are those measured by various authors in comets 8P, 9P, 21P, 73P, 103P, C/2000 WM1, C/2001 Q4, C/2002 T7, C/2009 P1, C/2012 F6 and C/2016 R2 at about the same epochs as our spectra [19–30]. The two outliers in four panels are comet C/2016 R2.

# 6 End notes

Supplementary Information is available for this paper.

Correspondence and requests for materials should be addressed to J. Manfroid

Email and orcid :

J. Manfroid jmanfroid@gmail.com 0000-0002-6930-2205

D. Hutsemékers d.hutsemekers@uliege.be

E. Jehin ejehin@uliege.be 0000-0001-8923-488X



Author contribution. JM analyzed the spectra and the coma profiles and wrote the main text. DH reduced the spectra, made the fluorescence model, computed the carbonyl properties and wrote section 4. EJ lead the UVES proposals and made most of the observations. All authors contributed to the discussion and the final text.

Acknowledgements. We thank Dr. P. van Hoof for useful discussions on the iron atomic data and their uncertainties. We thank Prof. R. Warin for suggesting that carbonyls could be at the origin of iron and nickel. JM, DH, and EJ are honorary Research Director, Research Director and Senior Research Associate at the F.R.S-FNRS, respectively.

# Figures

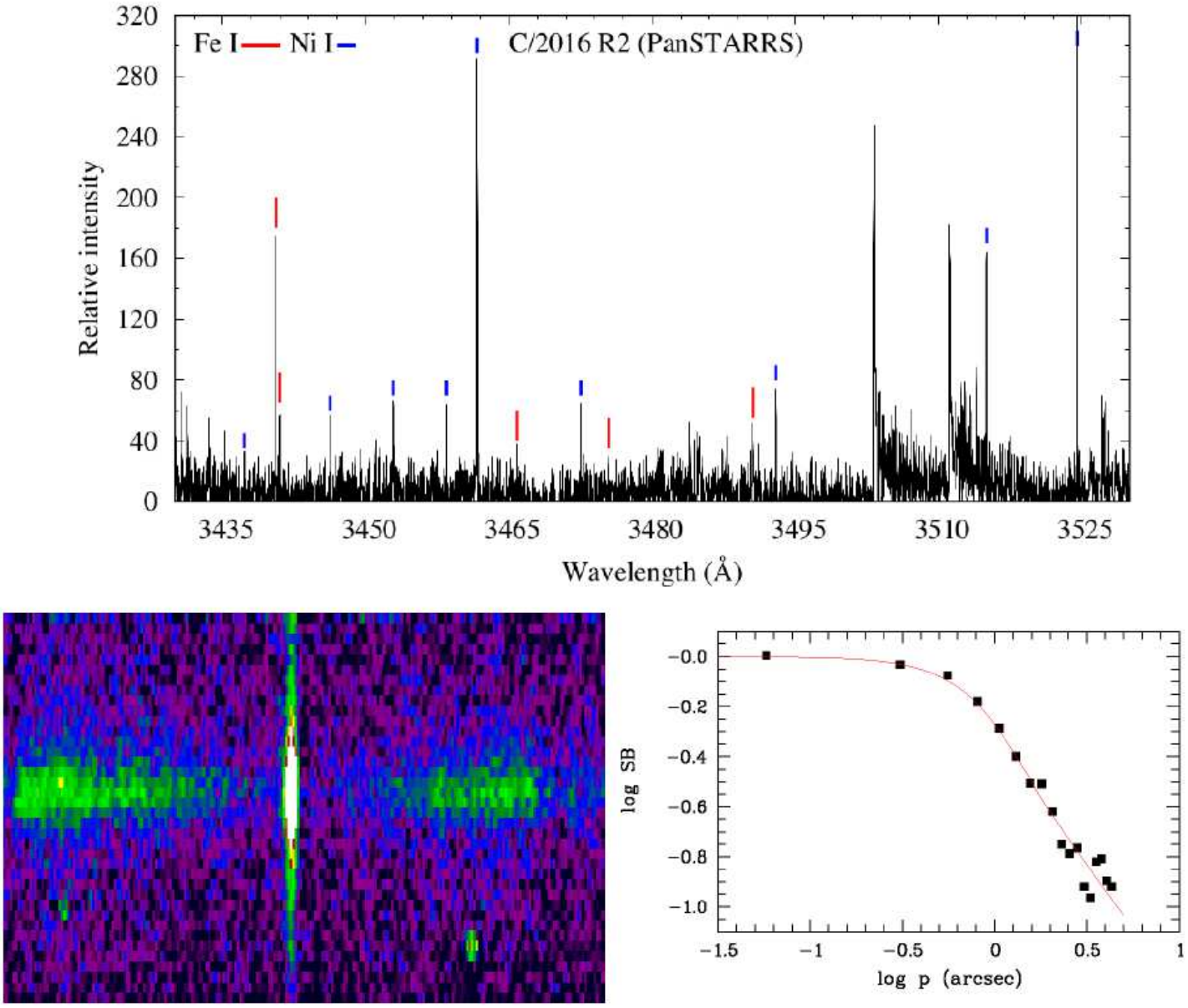


**Figure 1**

Observations of the Fe and Ni lines. Top. C/2016 R2 spectrum. Selected region showing many FeI and NiI lines in the spectrum of comet C/2016 R2 (PanSTARRS) obtained at the ESO Very Large Telescope. Bottom. The left panel shows the 2-dimensional spectrum of the FeI 3719 ˚A line in comet 103P/Hartley 2 on November 2010, at its closest approach to Earth at only 0.17 au. Wavelengths are along the horizontal axis and cover a range of 3 ˚A. The spatial dimension (vertical axis) extends over the entire height of the 10 arcsec slit (1230 km at the distance of the comet). The horizontal trace represents the reflected solar spectrum by the dust which shows a deep FeI absorption line. The spatial profile (right panel) plotted as a function of the projected nucleocentric distance p agrees well with a 1/p distribution of the surface

brightness and a 1.35 arcsec blurring corresponding to the seeing and the tracking imperfections. The NiI lines display the same profile.

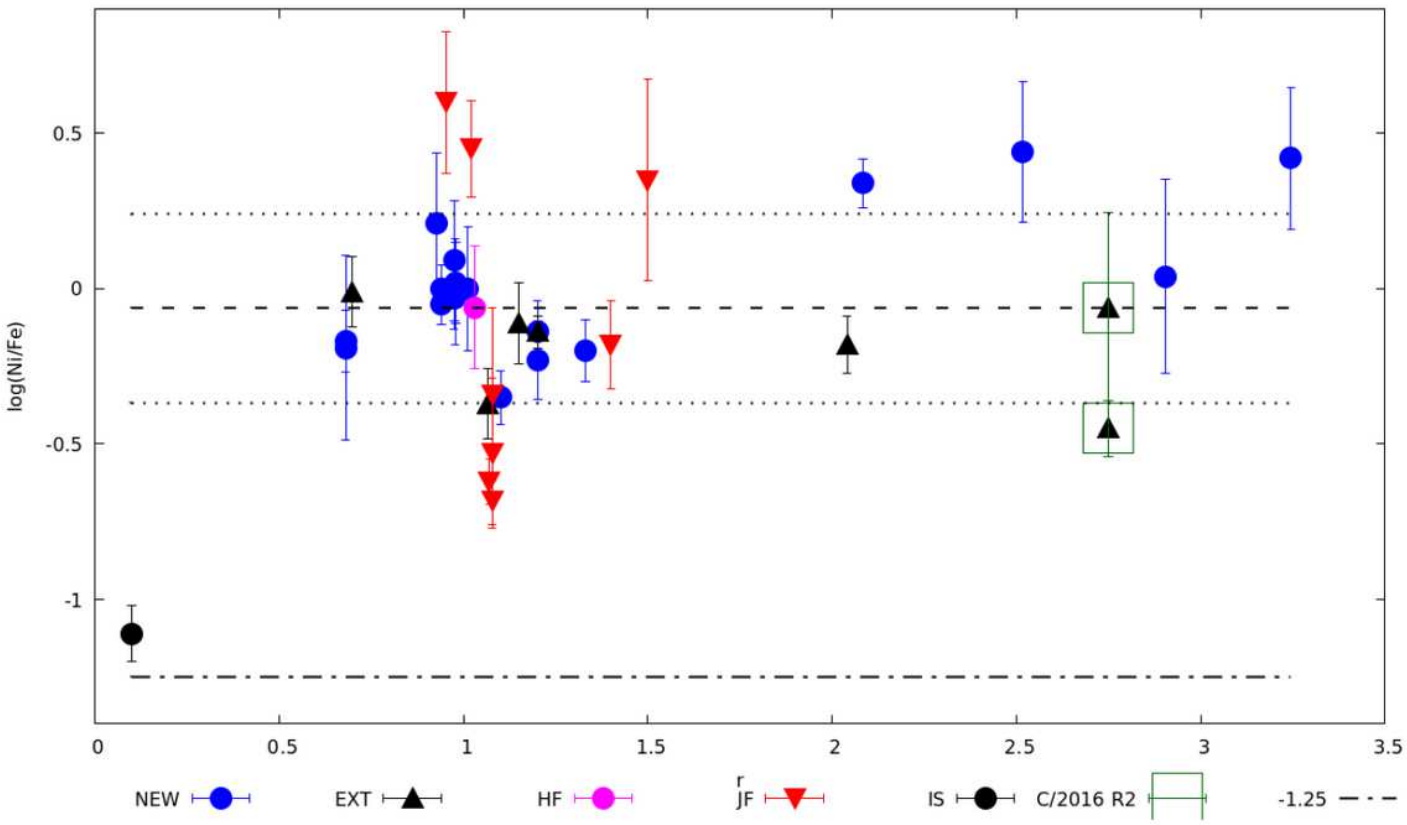


## Figure 2

Abundance ratios. Ni/Fe abundance ratios determined with the multilevel model for the comets of our sample. r is the heliocentric distance. Different symbols are used according to the dynamical class [30] : HFC (Halley Family) and JFC (Jupiter Family) correspond to ecliptic comets with short periods (< 200 years), EXT corresponds to external comets with semi-major axis a < 10000 au and NEW corresponds to external comets which directly come from the Oort cloud (a > 10000 au). The great comet C/1965 S1 (Ikeya-Seki) has been added. The horizontal dashed-dotted line indicates the solar value. The dashed and the dotted lines represent the sample average and the standard deviation.

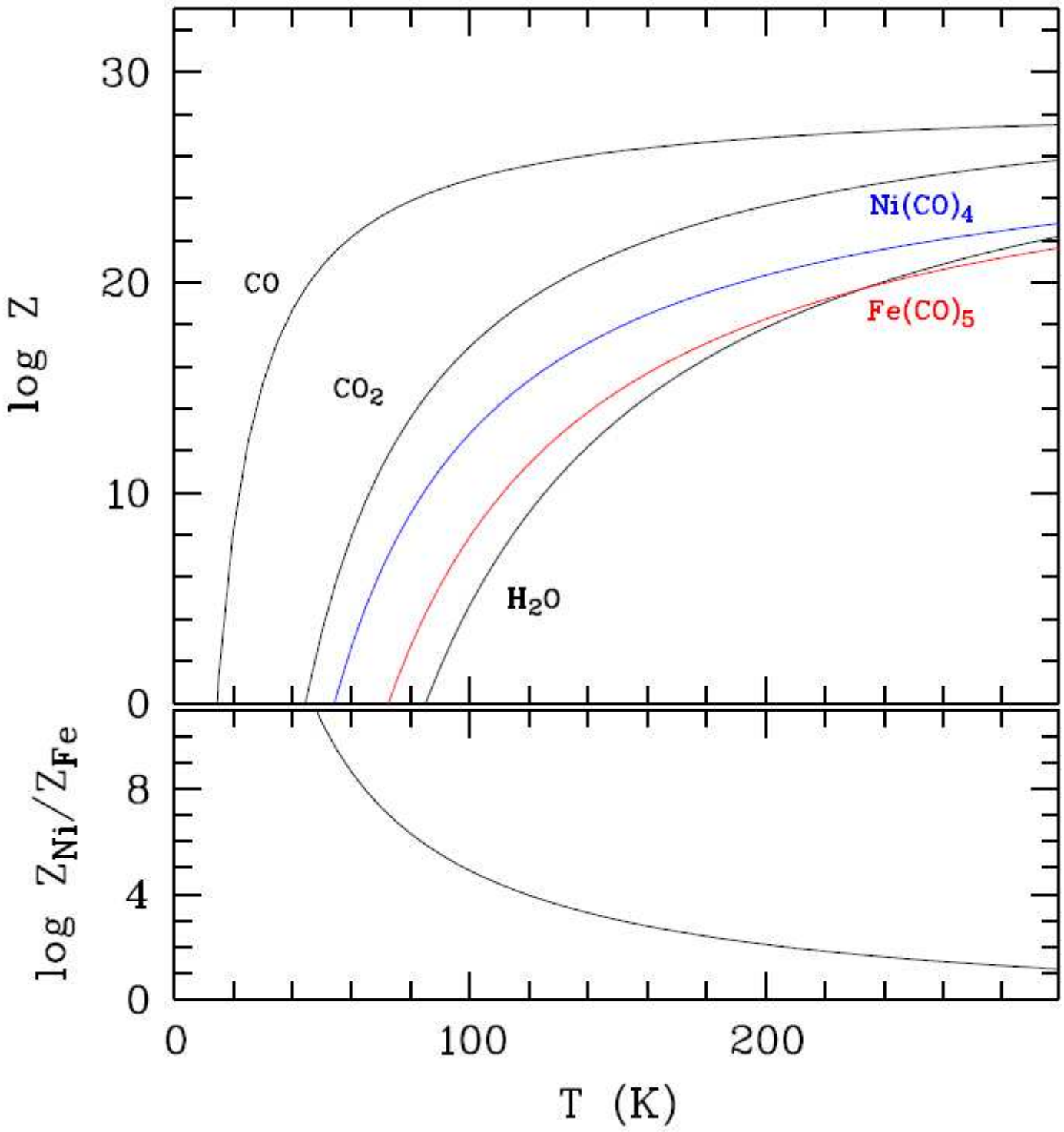


**Figure 3**

Sublimation of carbonyls. Top : the sublimation rate (in molecules cm−2 s−1) of iron and nickel carbonyls as a function of the temperature, compared to major species in comets. Bottom : the sublimation rate ratio Ni(CO)4 over Fe(CO)5.

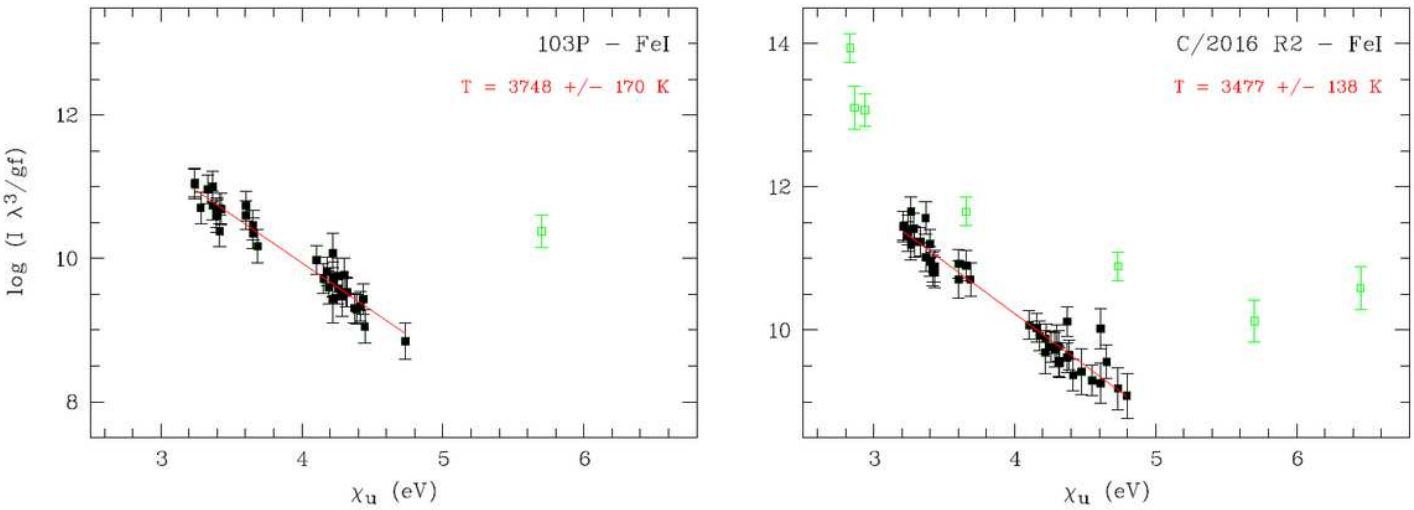


## Figure 4

Empirical determination of the excitation temperature. FeI emission lines observed in two representative comets are used. Outliers not considered in the fit are shown in green. For C/2016 R2 (and only for that comet) additional outliers were discarded through an iterative fit. Error bars account for the errors on the measured intensities and an uncertainty of log(gf) assumed to be 0.2 dex.

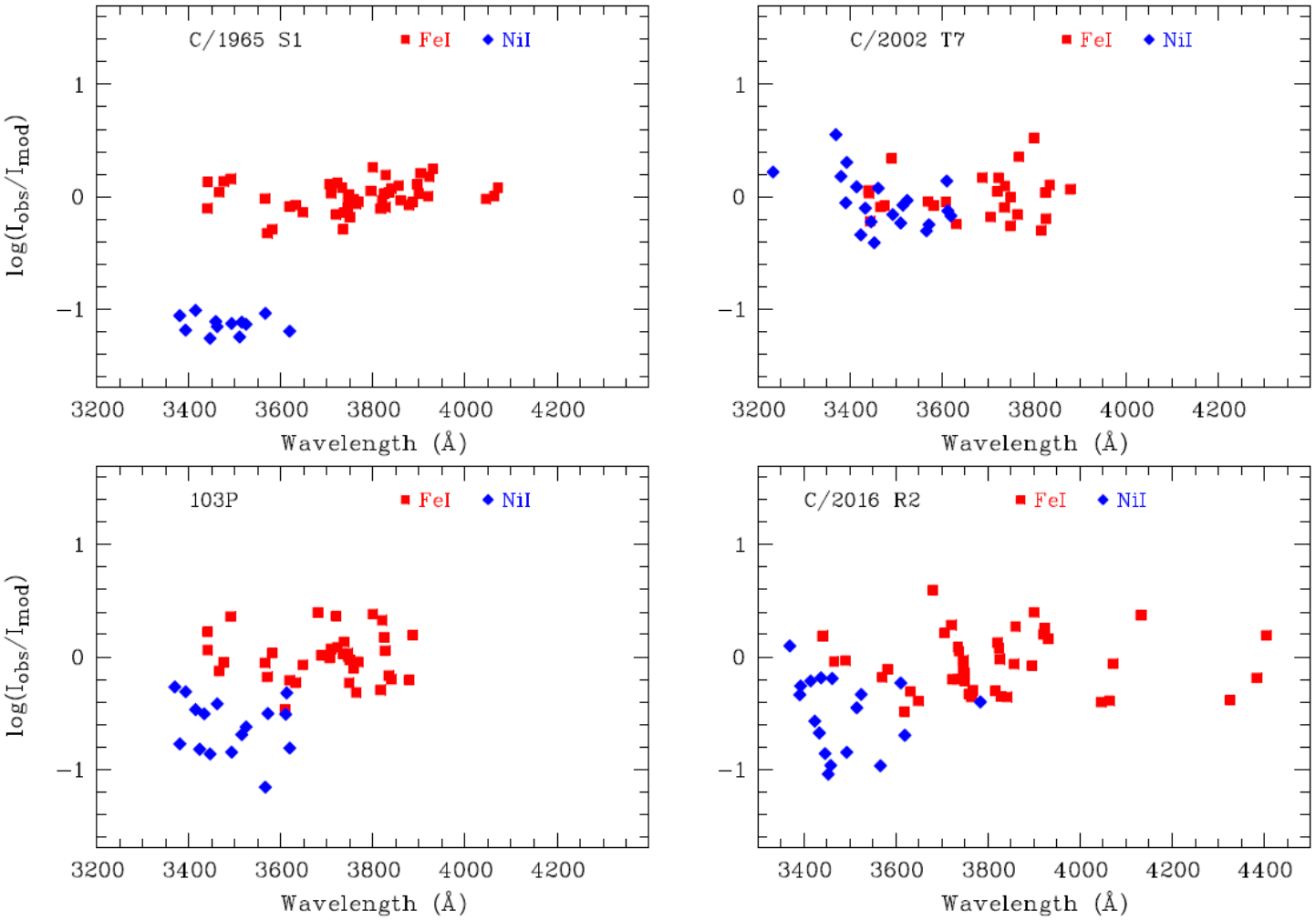


## Figure 5

Abundance ratio determination. The ratio log(Iobs/Imod) for the FeI (red) and NiI (blue) lines measured in four comets. The ratios have been shifted on the y-axis so that the mean of log(Iobs/Imod) is zero for FeI. The few outliers have been discarded. The difference of the means computed for FeI and NiI gives the log(Ni/Fe) abundance ratio (cf. Eq. 20).

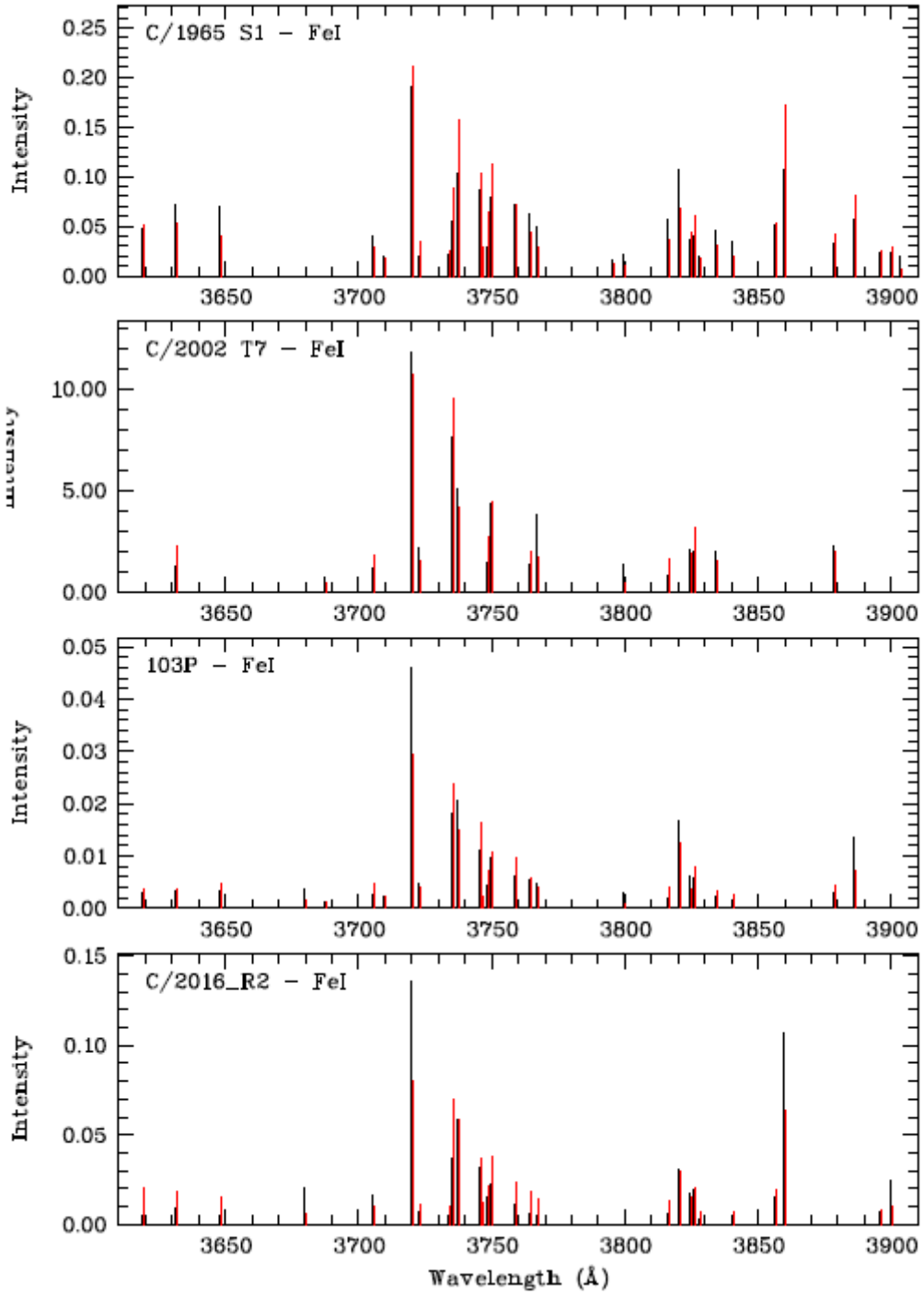


## Figure 6

Comparison of the observed and modeled spectra. A portion of the FeI spectrum is shown for four representative comets. Observed lines are in black; computed lines are in red, shifted by 0.7 ˚A for visibility.

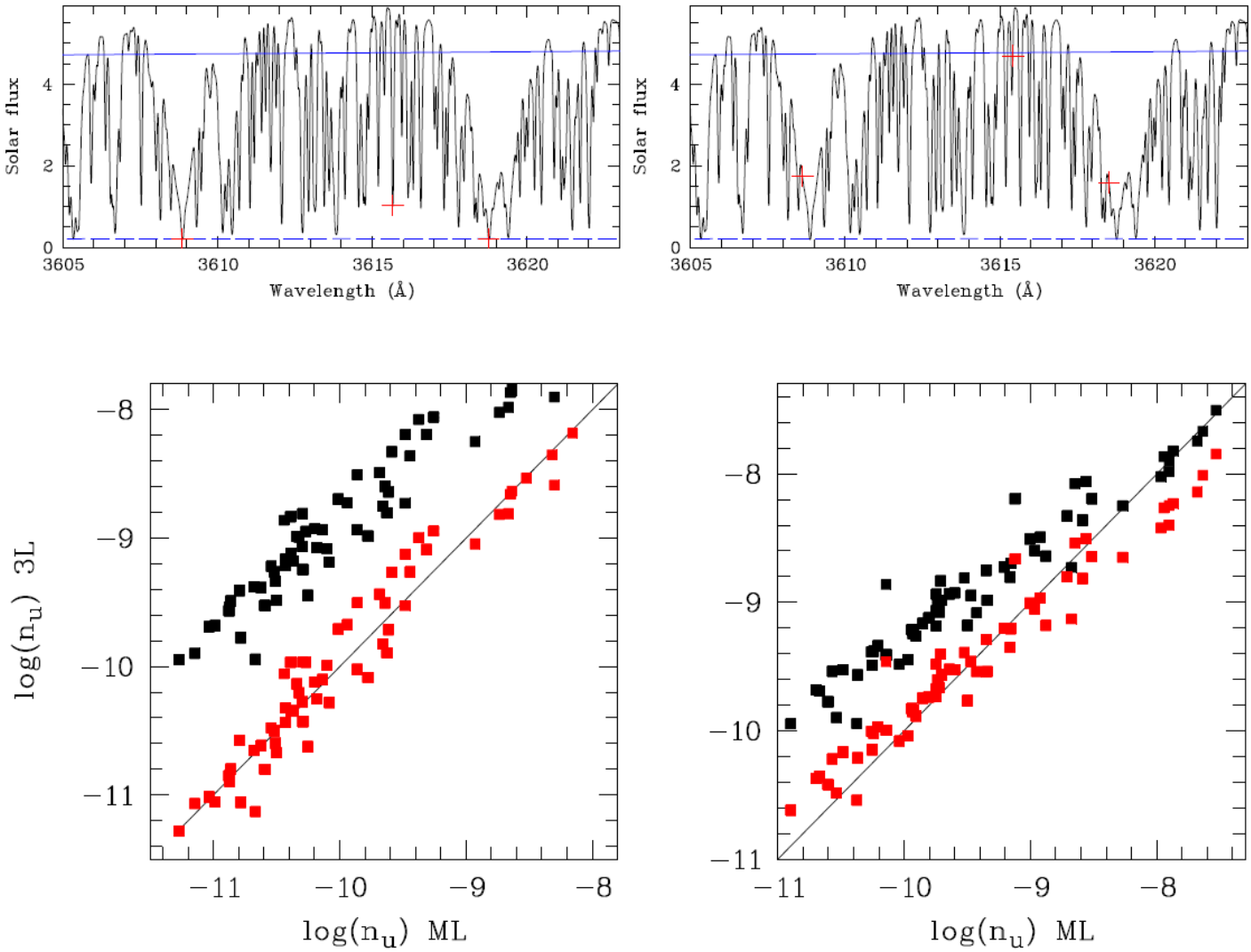


**Figure 7**

Effect of the solar spectrum. Top: Sample of the Kurucz solar spectrum. The red crosses indicate the value of the solar flux involved in three cometary FeI transitions. The solid blue line represents a blackbody spectrum with T = 5800 K, and the dashed blue line a blackbody spectrum with T = 4000 K. Cometary heliocentric velocities are equal to 0 km s−1 (left) and +20 km s−1 (right). The solar flux is given in arbitrary units. Bottom: Comparison of upper level populations computed for FeI with the 3-level and multilevel atomic models. Left: Black squares represent 3-level populations computed with a blackbody temperature of 5800 K (the color temperature of the Sun) while red squares represent 3-level populations computed with a temperature of 4400 K in better agreement with the mutilevel populations computed with the Kurucz solar spectrum . Right: Same as in the previous figure, but with the solar spectrum shifted by 20 km s−1. The red squares represent 3-level populations computed with a temperature of 5000 K.

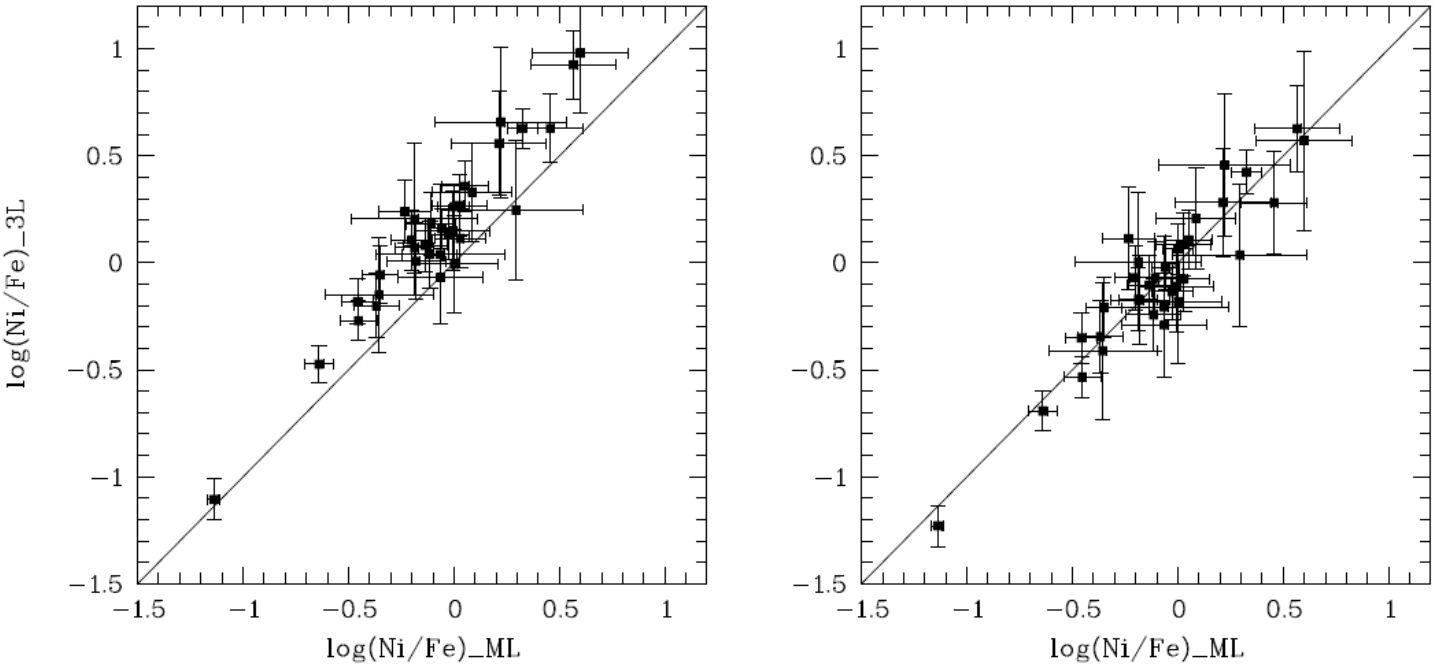


## Figure 8

Abundances from the two models. Comparison of log(Ni/Fe) abundances derived with the multilevel (ML) model and the 3-level (3L) model for the comets of our sample. Left: Assuming T (NiI) = T (FeI). Right: With T (NiI) = T (FeI)+180 K.

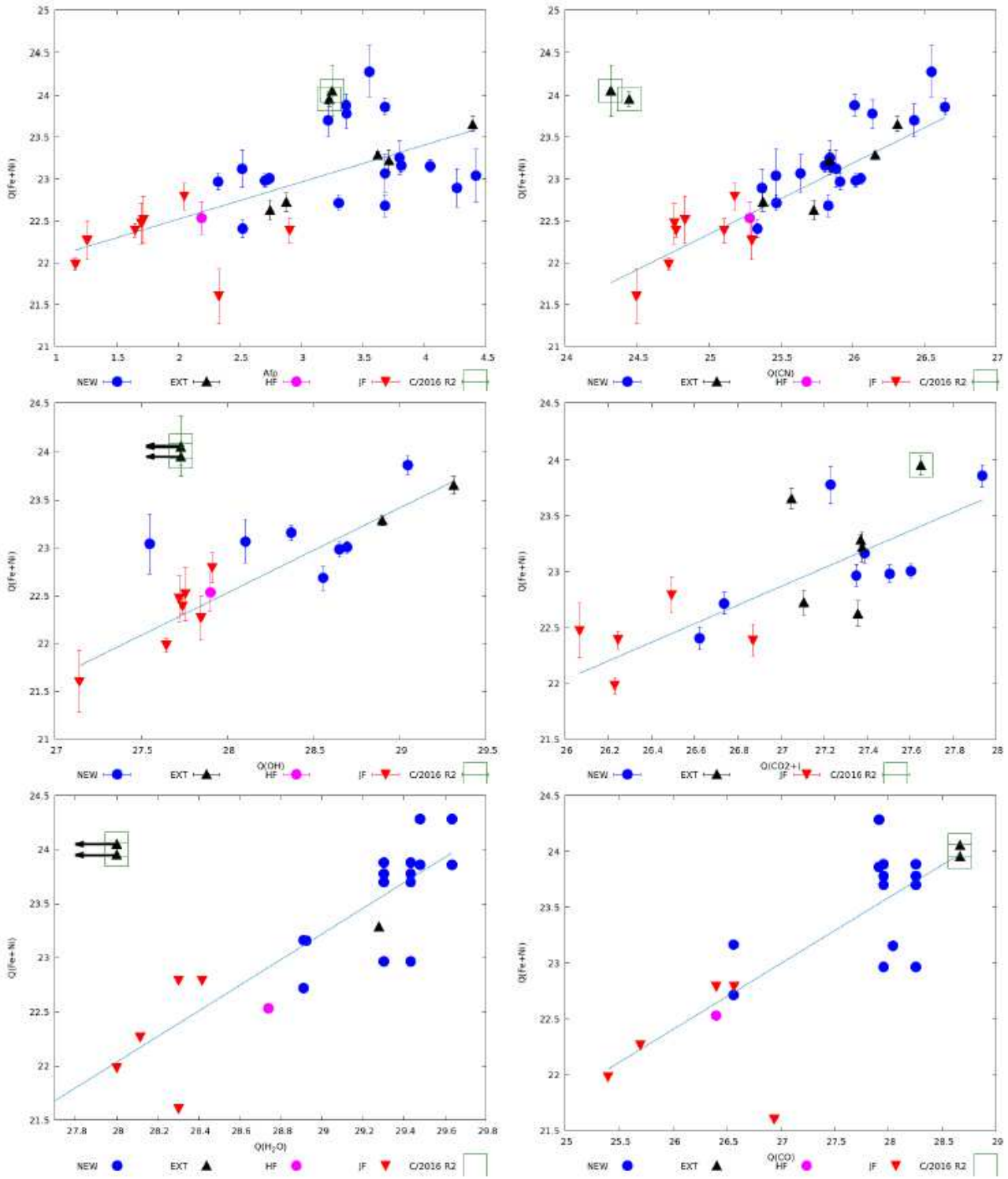


## Figure 9

Production rates correlations. Comparison between the logarithm of various production rates. Afρ is a proxy for the dust production rate (see text). The various cometary types are color coded according to their dynamical classification (see 1) : Halley Family, Jupiter Family, external and new comets. The OH and H2O values relative to comet C/2016 R2 are upper limits. The production rates of H2O and CO are those measured by various authors in comets 8P, 9P, 21P, 73P, 103P, C/2000 WM1, C/2001 Q4, C/2002 T7,

C/2009 P1, C/2012 F6 and C/2016 R2 at about the same epochs as our spectra [19–30]. The two outliers in four panels are comet C/2016 R2.

## Supplementary Files

This is a list of supplementary files associated with this preprint. Click to download.

- FNlines.csv